Synthesis of poly(L-Lactide)–Poly(-Caprolactone)–Poly(ethylene Glycol) Terpolymer Grafted onto Partially Oxidized Carbon Nanotube Nanocomposites for Drug Delivery

Karla J. González-Iñiguez , Edgar B. Figueroa-Ochoa , Antonio Martínez-Richa , Leonardo R. Cajero-Zul , Sergio M. Nuño-Donlucas *

Posted Date: 19 August 2024

doi: 10.20944/preprints202408.1347.v1

Keywords: nanocomposites; carbon nanotubes; poly(L-lactide); poly(-caprolactone); poly(ethylene glycol); methotrexate

 doi:10.20944/preprints202408.1347.v1

Article

Synthesis of Poly(L-Lactide)–Poly(ε-Caprolactone)–Poly(Ethylene Glycol) Terpolymer Grafted onto Partially Oxidized Carbon Nanotube Nanocomposites for Drug Delivery

Karla J. González-Iñiguez [1], Edgar B. Figueroa-Ochoa [2], Antonio Martínez-Richa [3], Leonardo R. Cajero-Zul [4] and Sergio M. Nuño-Donlucas [4,*]

[1] Doctorado en Ciencias en Ingeniería Química, Centro Universitario de Ciencias Exactas e Ingenierías, Universidad de Guadalajara, Guadalajara 44430, Mexico; josefina.gonzalez@academicos.udg.mx
[2] Departamento de Química, Centro Universitario de Ciencias Exactas e Ingenierías, Universidad de Guadalajara, Guadalajara 44430, Mexico; benjamin.figueroa@academicos.udg.mx
[3] Departamento de Química, Universidad de Guanajuato, Guanajuato 36050, Mexico; richa28@msn.com
[4] Departamento de Ingeniería Química, Centro Universitario de Ciencias Exactas e Ingenierías, Universidad de Guadalajara, Guadalajara 44430, Mexico; leocajero88@gmail.com (L.R.C.-Z.); gigio@cencar.udg.mx (S.M.N.-D.)
* Correspondence: gigio@cencar.udg.mx

Abstract: Nanocomposites prepared with a terpolymer of poly(L-lactide) (PLLA)–poly(ε-caprolactone) (PCL)–poly(ethylene glycol) (PEG) and partially oxidized carbon nanotubes ($CNTs_{po}$) were synthesized and characterized to evaluate their ability to act as an effective nanocarrier of the anticancer drug methotrexate. The homopolymers of PLLA and PCL were synthesized through ring-opening polymerization (ROP) and characterized through gel permeation chromatography (GPC). The PLLA–PCL–PEG terpolymers were synthesized through a four-step chemical route using oxalyl chloride as a linker agent and analyzed through ^{1}H-NMR, ^{13}C-NMR, and FT-IR spectroscopies. Also, the nanocomposites were characterized through FT-IR, ^{1}H-NMR, and X-ray photoelectron spectroscopy (XPS) spectroscopies and, using the differential scanning calorimetry (DSC) technique. XPS analysis revealed that $CNTs_{po}$ is grafted to PLLA–PCL–PEG terpolymer. Besides, evaluation through FT-IR and DSC strongly suggests that the $CNTs_{po}$ are preferentially oriented to the PCL-rich domains. The release tests exhibited a "burst effect" profile, which was more evident in the terpolymers than in the nanocomposites. Five models were used to assess the methotrexate in vitro release. For the nanocomposites, the best fit to the experimental data was obtained using the first-order model, whereas the results obtained from the Korsmeyer–Peppas model indicated that a Fickian diffusion drives the methotrexate release.

Keywords: nanocomposites; carbon nanotubes; poly(L-lactide); poly(ε-caprolactone); poly(ethylene glycol); methotrexate

1. Introduction

The design of novel stimuli-responsive drug delivery systems (DDS) that improve the efficiency of conventional drug delivery therapies responds to current demands in the medical field. DDS have the ability to activate drug release as a response to external stimuli. Different responsive stimuli can trigger drug delivery. Among these stimuli, those due to changes in the chemical environment in an aqueous medium (as changes in pH or conditions that favor the hydrolysis reaction) [1] gain special attention as they can be considered as a reference to prepare a polymeric carrier sensitive to the typic processes of the living organisms.

 doi:10.20944/preprints202408.1347.v1

Biocompatible polymers can be utilized as smart or external stimuli-responsive systems. For drugs delivered via systemic routes, it is desirable to develop a polymer-based drug carrier that can transport the drug to the target site and start the drug delivery under an external stimulus. But, preparing a new chemical polymeric structure that acts as sensitive carrier to external stimuli implies overcome a difficult task due to the associate undesired effects due to their interaction with living mater [2]. The goal is to use a polymer that works like a macromolecular shield protecting the drug on diverse biological environments that can affect the drug efficacy [3].

Among biodegradable and biocompatible polymers that are capable of protecting adsorbed drugs from degradation induced by the enzymes of the living bodies highlight three polymers: (i) polylactide (PLA; this abbreviation is typically used when the stereoregularity is not declared), (ii) poly(ε-caprolactone) (PCL), and (iii) poly(ethylene glycol) (PEG) [4].

PLA is a biodegradable biopolymer derived from renewable sources and is commercially available, but it has limited mechanical properties and low thermal resistance [5]. This hydrophobic, aliphatic polyester is used in tissue engineering [6], for preparing implants, drug delivery materials, and surgical sutures for the human body owing to its hydrolyzable capacity [7]. At an industrial level, PLA is synthesized in bulk through the ring-opening polymerization (ROP) of lactide (LA), which is a cyclic dimer of lactic acid [8]. Due to the chemical structure of LA having two chiral centers, two optical isomers of LA exist: D,D-lactide (D-LA) and L,L-lactide (L-LA). The products of the polymerization of these isomers are named poly(D-lactide) (PDLA) and poly(L-lactide) (PLLA), respectively. As a consequence of their optical purity, they have different thermal properties [9].

PCL is a biocompatible, biodegradable, bioresorbable biopolymer; it is easy to synthesize and popular in the biomedical field. The last is the consequence that, under physiological conditions, PCL experiments a slow hydrolysis by the cleavage of its ester groups [10]. This thermoplastic polyester is increasingly used to prepare drug-release materials and regenerative medicine implants as well as to develop new applications in the field of tissue engineering [11]. PCL is compatible with various drugs, such as antipsychotics, antibiotics, or anti-inflammatory agents [10]. Moreover, owing to its slow kinetic degradation and lack of bioactivity [12], it is suitable for preparation long-term DDS [13]. Because of their hydrophobic nature, lipophilic drugs can be homogeneously distributed in their polymeric chains [14], which is a factor that contributes to achieving a modulated drug release.

PEG is highly soluble in water, is FDA-approved, and is biocompatible. This polyether is widely available for preparing novel DDS owing to its low toxicity, nonimmunogenicity, nonantigenicity, and biological inertness [15,16]. The covalent addition of PEG to one or more molecules, known as PEGylation, is an efficient chemical approach used in drug delivery [17]. Carriers not modified with hydrophilic polymers are sensible to phagocytosis and the action of the reticuloendothelial system [3]. To prepare a “stealthy” system, the PEGylation can be employed to protect a hydrophobic carrier from opsonization.

Amphiphilic block copolymers formed by hydrophobic and hydrophilic segments of biodegradable and biocompatible polymers have gained considerable attention in drug delivery [18]. PLA, PCL, and PEG have been widely used to prepare nanoparticles of segmented copolymers, and their capacity to act as effective nanocarriers that achieve a controlled drug delivery has been investigated [19]. Special attention has been given to the nanocarrier–architecture relationship and its impact on systems that enable stable and safe drug release [20]. Several studies have reported the efficacy of PLA, PCL, and PEG-based segmented copolymers on drug delivery. Thus, the delivery of drugs (such as doxorubicin, an anticancer drug-) from the nanoparticles of PCL–PEG copolymers with a complex topology can be optimized by tuning the structure of these copolymers [21]. Poorly water-soluble drugs (such as silibinin, an anticancer agent) have been moderately encapsulated into a PEG–PLA-poly(α-benzylcarboxylate-ε-caprolactone) (PBCL) block copolymer to achieve cancer tumor-targeted delivery [22]. Amphiphilic block copolymers can be prepared through two typical routes: (i) via ring-opening copolymerization [23] and (ii) via a linker agent [24]. In this sense, oxalyl chloride has been used as an efficient linker. Its chemical structure has two acyl chloride groups that easily react with hydroxyl groups. Therefore, acyl chloride–capped polymers can be obtained after adding an excess of oxalyl chloride to polymers with terminal hydroxyl groups. After this, other

 doi:10.20944/preprints202408.1347.v1

polymers with hydroxyl end groups can react with the acyl chloride end group to obtain a block copolymer [25].

Although copolymers prepared using PLA, PEG, and PCL have relevant advantages for drug delivery, they also have limitations such as an initial "burst release" induced by the high crystallinity of the PCL [26]. The "burst release" phenomenon occurs when a sensitive polymer used as a drug carrier delivers high concentrations of the transported substance after coming into contact with the release medium. After an initial high delivery, a stable release can be achieved [27]. Some positive and negative consequences of "burst release" are known. For example, using modern antimicrobial drugs is desirable to achieve an "impact" dose in the initial stage, in which a high drug concentration is delivered to reduce bacterial growth in the shortest time possible. After this, in the second stage, it is necessary to obtain a gradual release rate [28]. However, to achieve a long-term optimal release, it is necessary to adjust the initial amount of drug released by reducing the "burst release" [29].

Carbon nanotubes (CNTs) are emerging DDS suitable for cancer treatment [30]. Owing to their large surface and cavity structures, CNTs can load high amounts of drugs [31]. Although they have outstanding properties, pristine CNTs are cytotoxic; to overcome this drawback, it is necessary to achieve adequate chemical functionalization [32]. Functionalized CNTs (f-CNTs) show suitable biocompatibility and living organisms can excrete them [33]. Furthermore, f-CNTs have the potential for use in the synthesis of polymer nanocomposites that can serve as nanocarriers. For this, the "grafting to" approach (in which the f-CNTs are attached to a well-defined polymer previously presynthesized [34]) is adequate for the preparation of a polymeric nanocarrier with excellent physicochemical properties.

Here, the synthesis and characterization of nanocomposites prepared with f-CNTs obtained from partially oxidized CNTs (in which hydroxyl and carboxyl groups were inserted) and a terpolymer of PLLA, PCL, and PEG prepared using oxalyl chloride as a linker agent is reported. These nanocomposites were synthesized to investigate their capacity to act as sensitive nanocarriers. Thus, a series of PLLAs and PCLs were synthesized through ROP and characterized by gel permeation chromatography (GPC). Pure PEG and the synthesized PLLAs and PCLs were studied through differential scanning calorimetry (DSC). The PLLA–PCL copolymers and PLLA–PCL–PEG terpolymers were synthesized using oxalyl chloride as a linker agent and characterized through the following spectroscopic techniques: Fourier-transform infrared (FT-IR), proton nuclear magnetic resonance (^{1}H-NMR), and ^{13}carbon nuclear magnetic resonance (^{13}C-NMR) as well as DSC. The PLLA–PCL–PEG terpolymers and their nanocomposites were analyzed by X-ray photoelectron spectroscopy (XPS). The characterization of the nanocomposites was completed through FT-IR and DSC. The capacity of releasing methotrexate (an anticancer drug) from the PLLA–PCL–PEG terpolymers and their nanocomposites was evaluated through ultraviolet-visible spectroscopy (UV-vis), and various mathematical models were used to fit the experimental data. Moreover, the ability of the nanocomposites to reduce the "burst release" phenomenon detected on the release tests of the pure PLLA–PCL–PEG terpolymers was assessed.

2. Materials and Methods

2.1. Materials

L-Lactide (L-LA) ((3*S*)-cis-3,6-dimethyl-1,4-dioxane-2,5-dione) (98%), ε-caprolactone (ε-CL) (97%), tin(II) 2-ethylhexanoate (stannous octoate, $SnOct_2$) (96%), 1,4-butanediol (BD) (99%), calcium hydride (>90%), triethylamine (ET_3N) (99.5%), toluene (ACS reagent) (99.5%), methanol (ACS reagent) (99.8%), dichloromethane anhydrous (99.8%), oxalyl chloride (OxCl) (98%), tetrahydrofuran (THF) (ACS grade), poly(ethylene glycol) (PEG) (M_n = 10000), phosphate-buffered saline (PBS) at pH 7.4, methotrexate (4-amino-10-methylfolic acid) MW = 454.44 g/mol, and ethanol (ACS reagent) were purchased from Sigma-Aldrich (Saint Louis, MO). Alumina boats were obtained from Alfa Aesar (Tewksbury, MA). Ethanol absolute (99.5%), hydrochloric acid (ACS reagent), and ferric nitrate nonahydrate ($Fe(NO_3)_3 \bullet 9H_2O$) were acquired from Golden Bell (Guadalajara, Mexico). Petroleum ether (ACS reagent) (distillation range: 20°C (293.15 K) – 60°C (333.15 K)) was purchased from Almacén de Drogas la Paz (Guadalajara, Mexico). Nitrogen gas (99.99%) was obtained from INFRA

 doi:10.20944/preprints202408.1347.v1

(Guadalajara, Mexico). Argon gas (99.998%) was provided by Linde (Guadalajara, Mexico). Deionized and bi-distilled water was purchased from Productos Selectropura (Guadalajara, Mexico). The chemical reagents mentioned above were used without purification, except for ε-CL which was dried with calcium hydride under constant stirring for 48 h before use. The flask, in which the mixture of ε-CL/calcium hydride was deposited was connected to a Schlenk line under a nitrogen atmosphere. Then, an exhausting refilling process was repeated three times to separate the wet calcium hydride from the dry ε-CL. The dry ε-CL was deposited into a container and placed in a desiccator until use. The amount of water contained in unpurified BD was determined using the Karl Fischer method, resulting in 16.3 wt.%. The measurement was repeated three times. Therefore, the BD used in this work was named wet BD.

2.2. Preparation, Purification, and Chemical Modification of the Prepared CNTs

The CNTs were synthesized using the chemical vapor deposition (CVD) method with Fe as a catalyst and ethanol as a carbon source. A detailed description of the synthesis procedure was previously reported by our research group elsewhere [35]. The prepared CNTs were purified using a solution of HNO_3 (37.5 wt.%) in water (1:3 v/v). The purified CNTs were repeatedly washed with bi-distilled water until a pH of 7 was achieved and oven-dried at 50°C (323.15 K). The detailed purification pathway was previously reported elsewhere [36]. The purified CNTs were named $CNTs_{puri}$. $CNTs_{puri}$ were chemically functionalized through an oxidation process. For this, 1 g of $CNTs_{puri}$ was deposited into the 250-mL glass of Soxhlet equipment. Subsequently, 140 mL of 4 M nitric acid solution was aggregated. The mixture was heated until the boiling point was reached and kept under reflux for 5 h. The product (partially oxidized CNTs) was named $CNTs_{po}$ and was recovered through centrifugation. Finally, the $CNTs_{po}$ were washed with bi-distilled water several times until a pH of 7 was obtained and oven-dried at 50°C (323.15 K) for 72 h. The dry $CNTs_{po}$ were stored in a desiccator until use. Hereby, carbonyl, hydroxyl, and carboxyl chemical groups were inserted on the walls of the $CNTs_{po}$.

2.3. Synthesis of the PLLA–PCL–PEG Terpolymers

PLLA–PCL–PEG terpolymers were synthesized following a chemical path of four steps. First, a PLLA homopolymer was synthesized through ROP using wet BD as an initiator and $SnOct_2$ as a catalyst. The polymerization reaction was carried out in a 150-mL two-neck round-bottom glass flask previously dried at 60°C (333.15 K) for 24 h. L-LA (15 g), wet BD and $SnOct_2$ at specific amounts, and a stirring bar (previously dried at 50°C (323.15 K) for 24 h) were placed into the flask connected to a reflux condenser. The flask was partially submerged in an oil bath maintained at 110°C (383.15 K). Polymerization was performed under a nitrogen atmosphere with stirring for 1 h. After the reaction was completed, the flask was cooled to room temperature. To purify the prepared product, it was dissolved in 20 mL of dichloromethane and poured dropwise into 60 mL of petroleum ether to induce precipitation. The product was maintained at room temperature for 3 h, and the precipitate was recovered through centrifugation. Subsequently, it was washed with methanol and dried at 45°C (318.15 K) until a constant weight was reached. Four lineal PLLAs were synthesized at the same molar ratio of [L-LA]/[$SnOct_2$] = 300/1 but at four different molar ratios of [L-LA]/[wet BD], which were named (i) PLLA 1 obtained at [L-LA]/[wet BD] = 30/1, (ii) PLLA 2 prepared at [L-LA]/[wet BD] = 40/1, (iii) PLLA 3 synthesized at [L-LA]/[wet BD] = 50/1, and (iv) PLLA 4 manufactured at [L-LA]/[wet BD] = 60/1. The expected product of this synthesis is a PLLA-diol. Second, a series of PCLs were synthesized through ROP again. For this, 10 g of dry ε-CL and a dry stirring bar were placed in a 150-mL two-neck round-bottom glass flask previously dried. Then, specific amounts of wet BD and $SnOct_2$ as well as a dry stirring bar were added, and the flask was partially submerged in an oil bath at 110°C (383.15 K). The reaction was carried out, maintaining constant nitrogen bubbling with stirring for 1 h. After the reaction was completed, the flask was cooled to room temperature. The reaction product was purified by dissolving it in 20 mL of dichloromethane and then precipitated by adding 60 mL of petroleum ether. The prepared PCL was recovered through centrifugation. Thereafter, the prepared PCL was oven-dried at 45°C (318.15 K) until a constant weight was reached.

 doi:10.20944/preprints202408.1347.v1

Four lineal PCLs were prepared, maintaining the same molar ratio [ε-CL]/[$SnOct_2$] = 300/1 but different molar ratios of [ε-CL]/[wet BD]. The synthesized PCLs were named PCL 1, PCL 2, PCL 3, and PCL 4, which were synthesized at [ε-CL]/[wet BD] = 30/1, 40/1, 50/1, and 60/1, respectively. Following this procedure, PCL diol species would be synthesized. Third, the linear segmented copolymers of PLLA–PCL were synthesized using OxCl as a linker agent following a two-stage procedure. The four prepared PCLs and the PLLA 1 were chosen to synthesize the PLLA–PCL copolymers. In the first stage, a sample of PLLA 1 reacted with OxCl to prepare a prepolymer. The synthesis was performed in a two-neck round-bottom glass flask with a septum inlet of 50 mL previously dried at 50°C (323.15 K) for 12 h. One neck was connected to a reflux condenser, and on the other neck, a septum was adjusted. A steel cannula was inserted into the septum for bubbling nitrogen. A certain mass of PLLA 1 was dissolved in 10 mL of dichloromethane, and the dissolution was placed in the flask, which was partially submerged in an oil bath at 35°C (308.15 K). Then, 30 μL of ET_3N dissolved in 5 mL of dichloromethane was added to this flask. Separately, 70 μL of OxCl dissolved in 5 mL of dichloromethane was added dropwise. The mixture was maintained under continuous agitation and with nitrogen bubbling for 1 h. Under these conditions, a chemical reaction between the hydroxyl groups of PLLA 1 and chloride acyl groups of OxCl could be carried out to obtain a prepolymer. In the second step, the synthesis of PLLA–PCL copolymers was carried out. For this, immediately after finishing the first stage, a certain mass of one PCL dissolved in 5 mL of dichloromethane was added to the mass of the prepolymer, and the copolymerization reaction started. The reaction was carried out for 1 h. The masses of PLLA 1 and the PCL used were calculated, maintaining a ratio of 2 moles of the end groups of PCL to 1 mole of the end groups of PLLA 1. After the reaction time had elapsed, the reaction mixture was cooled to room temperature, which was kept unchanged for 24 h, and then purified. For this, a mixture of 15 mL of dichloromethane and 15 mL of toluene was added to dissolve the PCL that did not react. The mixture was stirred for 15 min, filtrated, and then oven-dried at 45°C (318.15 K) until a constant weight was achieved. Subsequently, the dry solid was dissolved in 15 mL of dichloromethane and precipitated with the addition of 45 mL of petroleum ether. The solid obtained (purified PLLA–PCL copolymer) was recovered and oven-dried until a constant weight was achieved. Four PLLA–PCL copolymers were synthesized: (i) PLLA–PCL 1 prepared with PLLA 1 and PCL 1, (ii) PLLA–PCL 2 obtained with PLLA 1 and PCL 2, (iii) PLLA–PCL 3 manufactured with PLLA 1 and PCL 3, and (iv) PLLA–PCL 4 synthesized with PLLA 1 and PCL 4. Fourth, the PLLA–PCL–PEG terpolymers were obtained through a chemical reaction between the PLLA–PCL copolymers and PEG. Again, a chemical route of two stages was followed. OxCl was used as a linker agent. In the first stage, a certain mass of the PLLA–PCL copolymer was treated with OxCl to synthesize a precursor of the terpolymer. To perform the synthesis, a 50-mL two-neck round-bottom glass flask immersed in an oil bath at 35°C (308.15 K) was used. Initially, a certain mass of one PLLA–PCL copolymer was dissolved in 10 mL of dichloromethane, and dissolution was deposited in the flask. Then, 30 μL of ET_3N dissolved in 5 mL of dichloromethane was added. Another solution of 70 μL of OxCl dissolved in 5 mL of dichloromethane was added. The mixture was reacted for 1 h under a nitrogen atmosphere. In this way, the hydroxyl end groups of the PLLA–PCL copolymer can react with one acyl chloride group of OxCl. In the second stage, complete preparation of the terpolymers was achieved. For this, elapsed the reaction time of the first stage, a certain mass of PEG dissolved in 5 mL of dichloromethane was added to the precursor, and the mixture was maintained under nitrogen bubbling for 1 h. The mass of the PEG added was calculated, maintaining a molar ratio of 2 moles of the end groups of PEG by 1 mole of the end groups of the PLLA–PCL copolymer, under the hypothesis that this copolymer has a chemical structure composed of three segments: PCL–PLLA–PCL. The reaction product was cooled to room temperature and then purified after 24 h. Purification was carried out by washing the product prepared with methanol to dissolve the PEG that did not react. Then, the purified product (PLLA–PCL–PEG terpolymer) was oven-dried at 45°C (318.15 K) until constant weight was reached. The prepared terpolymers were named PLLA–PCL–PEG 1, PLLA–PCL–PEG 2, PLLA–PCL–PEG 3, and PLLA–PCL–PEG 4, which were synthesized by the chemical reaction between PLLA–PCL 1, PLLA–PCL 2, PLLA–PCL 3, and PLLA–PCL 4 with

 doi:10.20944/preprints202408.1347.v1

PEG, respectively. Scheme 1 shows the expected chemical structure of the prepared PLLA–PCL–PEG terpolymers by the described chemical path.

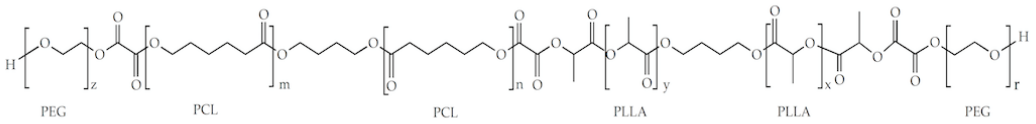

Scheme 1. Expected chemical structure of the prepared PLLA-PCL-PEG terpolymers.

2.4. Synthesis of PLLA–PCL–PEG/CNT$_{po}$ Nanocomposites

To prepare the PLLA–PCL–PEG/CNT$_{po}$ nanocomposites a certain mass of each PLLA–PCL–PEG terpolymer was dissolved in THF. In this solution, 1.0 wt.% or 0.5 wt.% of CNTs$_{po}$ was added. The dispersion obtained was placed in a Petri dish and sonicated for at least 30 min at 40°C (313.15 K) until the solvent evaporated. The Petri dish was heated in an oven at 45°C (318.15 K) to eliminate the solvent residual. Subsequently, the prepared and dried nanocomposites were stored in a desiccator. Table 1 lists the names of the PLLA–PCL–PEG terpolymers used as polymer matrices of the prepared PLLA–PCL–PEG/CNT$_{po}$ nanocomposites and the contents (in wt.%) of CNTs$_{po}$ of each nanocomposite.

Table 1. Identification legends of the PLLA-PCL-PEG terpolymers, the PLLA-PCL-PEG/CNTs$_{po}$ nanocomposites and the content of CNTs$_{po}$ (wt.%) in each nanocomposite.

Legend assigned to the PLLA-PCL-PEG/CNTs$_{po}$ nanocomposites prepared	Name of the PLLA-PCL-PEG terpolymer used as the polymer matrix of a nanocomposite	Content of CNTs$_{po}$ (wt.%)
NC 1	PLLA-PCL-PEG 2	1.0
NC 2	PLLA-PCL-PEG 2	0.5
NC 3	PLLA-PCL-PEG 4	1.0
NC 4	PLLA-PCL-PEG 4	0.5

2.5. Characterization of CNTs$_{po}$, PLLA–PCL–PEG Terpolymers, and PLLA–PCL–PEG/CNT$_{po}$ Nanocomposites

The prepared CNTs$_{po}$, synthesized PLLA and PCL homopolymers, homopolymer PEG, synthesized PLLA–PCL copolymers, and PLLA–PCL–PEG terpolymers, as well as the obtained PLLA–PCL–PEG/CNT$_{po}$ nanocomposites were characterized using the techniques described as follows.

2.5.1. Characterization of the Functionalized CNTs

The amount of carboxyl and hydroxyl groups inserted on the walls of the CNTs$_{po}$ was determined using two methods reported elsewhere, respectively [35,37]. Both methods were based on a back titration of a hydrochloric acid solution. This solution reacts with the excess of a sodium hydroxide solution to determine the amount of hydroxyl groups or the excess of a sodium bicarbonate solution to calculated the amount of carboxyl groups. The determinations were conducted by mass of CNTs$_{po}$.

2.5.2. GPC

GPC was employed to determine the molar masses of the synthesized polymers and their molar mass distributions. For this, dilute solutions of each sample were prepared. These solutions were

 doi:10.20944/preprints202408.1347.v1

prepared by dissolving 10 mg of the sample in 2 mL of THF. Subsequently, they were filtered through a 0.45-mm pore and 13-mm diameter filter (GHP Acrodisc Gelman (St. Louis, USA)). The measurements were made in a Waters model 2414 chromatograph provided with Waters Styragel columns, which cover the range of 500–300,000 Da, and a refraction index detector. All tests were conducted using THF as an eluent (1.0 mL/min) at 30°C (303.15 K). Calibration was performed using polystyrene standards. The data treatment was performed using Empower software (version 2).

2.5.3. Proton and Carbon-13 Nuclear Magnetic Resonance (^{1}H- and ^{13}C-NMR)

The ^{1}H- and ^{13}C-NMR spectra of the PLLA–PCL copolymers and the PLLA–PCL–PEG terpolymers were recorded at room temperature using Bruker Avance III 500 (MHz) (Billerica, USA). Chemical shifts (ppm) were relative to the remaining nondeuterated chloroform signal (from $CDCl_3$) and used as an internal reference for ^{1}H NMR spectroscopy. The peaks for PLLA moiety appeared at 1.60 and 5.2 ppm due to the (–C**H**$_3$) and (–C**H**–) groups, respectively, in all samples. The peaks for PCL appeared at 4.0 ppm [–(CH$_2$)$_4$C**H**$_2$OC(O)–]$_n$, 2.3 ppm (–(CH$_2$)$_4$C**H**$_2$COO–), 1.6 ppm (–(CH$_2$C**H**$_2$CH$_2$C**H**$_2$CH$_2$COO–), and 1.35 ppm (–CH$_2$CH$_2$C**H**$_2$CH$_2$CH$_2$COO–). The end groups due to the PLLA methine end group (–CH$_3$C**H**OH) were seen at 4.4 ppm. This peak is superimposed with other peaks. The peaks for the ε-CL end group –C**H**$_2$OH appeared at ca. 3.65 ppm, whereas those for PEG methylene (OC**H**$_2$CH$_2$) appeared at ca. 3.60 ppm.

The ^{13}C-NMR spectra were also recorded on Bruker Avance III 500 (MHz) (Billerica, USA). The peaks for PLLA moiety appeared at 16.7, 69.1, and 169.6 ppm due to the (–**C**H$_3$), (–**C**H–), and (**C**=O) groups, respectively, in all samples. The peaks for PCL appeared at 64.2 ppm [–(CH$_2$)$_4$**C**H$_2$OC(O)–]$_n$, 34.1 ppm (–(CH$_2$)$_4$**C**H$_2$COO–), 28.3 ppm (–(CH$_2$**C**H$_2$CH$_2$CH$_2$CH$_2$COO–), 24.5 ppm (–(CH$_2$CH$_2$CH$_2$**C**H$_2$CH$_2$COO–), 25.5 ppm (–CH$_2$CH$_2$**C**H$_2$CH$_2$CH$_2$COO–), and 173.6 ppm for ester carbonyl. The signal peak for PEG methylene (O**C**H$_2$CH$_2$) was seen at 70.5 ppm.

2.5.4. Fourier-Transform Infrared Spectroscopy (FT-IR)

The vibrational behaviors of the CNT$_{po}$, PLLA, PCL, and PEG homopolymers, PLLA–PCL–PEG terpolymers, and PLLA–PCL–PEG/CNT$_{po}$ nanocomposites were analyzed via FT-IR. For this, a spectrophotometer model Spectrum One of Perkin Elmer, was used. To obtain the spectra, all samples were dried in a vacuum oven at 50°C (323.15 K) until a constant weight was achieved. Similarly, KBr was dried in a vacuum oven at 100°C (373.15 K) for 24 h. Then, dry samples were mixed with dry KBr (1 mg of sample by 200 mg of KBr), and pellets were obtained by compression. The spectra were recorded from 4000 to 450 cm^{-1} and are an average of 50 scans to reduce the signal/noise ratio and were obtained at a resolution of 2 cm^{-1}.

2.5.5. XPS

The PLLA–PCL–PEG terpolymers and PLLA–PCL–PEG/CNT$_{po}$ nanocomposites were investigated through XPS. The analysis was conducted in a system formed by XR 50M monochromatic Al $K\alpha_1$ ($h\nu$ = 1468.7 eV) X-ray source, and a Phoibos 150 spectrometer, which was equipped with a one-dimensional detector 1D-DLD provided by SPECS (Berlin, Germany). For the measurements, the samples were mounted on a steel sample holder using a double-sided copper tape to avoid interference from the carbon tape and dried in a vacuum oven for 24 h. Then, the samples were placed into the prechamber. The measurements were recorded at a base pressure of 4.2×10^{-10} mbar, an electron takeoff angle of 90° at 150 W, a pass energy of 10 eV, and a step size of 0.1 eV. To compensate for the charge on samples, a flood gun was used. The XPS spectra recorded were shifted using the reference of the C–C binding energy position.

2.5.6. DSC

Thermal characterization of the PLLA, PCL, and PEG homopolymers, PLLA–PCL–PEG terpolymers, and PLLA–PCL–PEG/CNT$_{po}$ nanocomposites was performed using calorimeter model Q-100 (TA Instruments). DSC thermograms were obtained with a dynamic heating program in a

 doi:10.20944/preprints202408.1347.v1

temperature range of −70°C (203.15 K) to 200°C (473.15 K) following a heating rate of 10°C (10 K)/min. An inert atmosphere was kept feeding a flow rate of nitrogen at 50 mL/min to the sample camera. The masses of the samples were in the range of 5 to 5.5 mg. Aluminum pans were used to encapsulate the samples. Two scans were recorded, and the second scan was reported. The glass transition temperature (T_g) of all the materials analyzed was determined using the mid-point criteria.

2.5.7. Ultraviolet–Visible (UV–Vis) Spectroscopy

To assess the methotrexate in vitro release from the tablets of the PLLA–PCL–PEG 2 and PLLA–PCL–PEG 4 terpolymers as well as NC 1, NC 2, NC 3, and NC 4 nanocomposites, UV–vis spectroscopy was employed. For this, a spectrometer model Evolution 220 (Thermo Fisher Scientific) was utilized. The tablets were prepared by compression mixing a certain mass of the terpolymers or the mentioned nanocomposites with the methotrexate. The total masses of the tablets were in the range of 50 to 85 mg. The mass ratio of terpolymer or nanocomposite to methotrexate was 10/1. The tablets obtained had a thickness of 4 mm. Each prepared tablet was introduced in a dialysis membrane (SpectrPor, MWCO 3500 Da), and deposited in a 500 mL-beaker. After this, 200 mL of PBS buffer at pH 7.4 was added. Then, 4 mL of ethanol was added to inhibit the formation of aggregates of the drug methotrexate [38]. The mixture obtained deposited in the beaker was introduced in a dark camera to protect the methotrexate (a photosensitive substance) of the visible light at 37°C (310.15 K). The mixture was maintained under constant stirring at 250 rpm. Samples (1 mL) of this mixture were taken in the range of 0 to 96 h. After each volumetric sample was withdrawn, the same volume of PBS buffer was added. The evolution of methotrexate release was evaluated by determining the methotrexate concentration, evaluating the absorbance at 302 nm as a function of the time using a calibration curve prepared with solutions of methotrexate in PBS. Each release test was repeated twice.

3. Results and Discussion

3.1. Functionalization of the CNTs

Quantification of the amount of the hydroxyl and carboxyl groups inserted on the walls of the $CNTs_{po}$ was performed using the aforementioned experimental methods. The carboxyl groups represent 33 wt.% per gram of $CNTs_{po}$, whereas the hydroxyl groups represent 15 wt.% estimated per gram of $CNTs_{po}$.

3.2. Characterization by GPC of the Homopolymers of PLLA and PCL

The GPC results of the homopolymerization of L-LA and ε-CL and the yield of both polymerizations are listed in Table 2. These results were obtained from the GPC patterns of the PLLA and PCL synthesized. A high yield (≥ 90%) of all homopolymerization reactions was obtained. As expected, the weight-average molar mass (M_w) of both linear PLLAs and PCLs increased as the molar ratio [L-LA]/[wet BD] and [ε-CL]/[wet BD] reached higher values. The polydispersity index (PDI = M_w/M_n) of the synthesized PLLAs had values close to 1.0, whereas the PDI of the prepared PCLs had slightly larger values.

Table 2. GPC results and yield of the homopolymerization of L-LA and ε-CL both polymer precursors were denominated here as M.

Homopolymer	Molar ratio of [M]/[wet BD]	M_w (g/mol^{-1})	M_w/M_n	Yield (%)
PLLA 1	30/1	24670	1.07	90
PLLA 2	40/1	31110	1.08	92
PLLA 3	50/1	34250	1.09	95
PLLA 4	60/1	34800	1.07	90
PCL 1	30/1	10280	1.07	90
PCL 2	40/1	25650	1.10	90

 doi:10.20944/preprints202408.1347.v1

PCL 3	50/1	32330	1.16	93
PCL 4	60/1	35370	1.11	91

3.3. Analysis of the Chemical Structure of the PLLA–PCL Copolymers, PLLA–PCL–PEG Terpolymers, and PLLA–PCL–PEG/CNT$_{po}$ Nanocomposites

The ^{1}H-NMR spectrum of the PLLA–PCL 2 copolymer is shown in Figure 1. The PLLA/PCL ratio was determined through ^{1}H NMR spectroscopy using the integral values for the signal assigned to the repeating groups in the synthesized copolyesters. In the case of PLLA, the methine group at δ = 5.2 ppm was used, whereas, for PCL, the ε-methylene group at δ = 4.0 ppm was used.

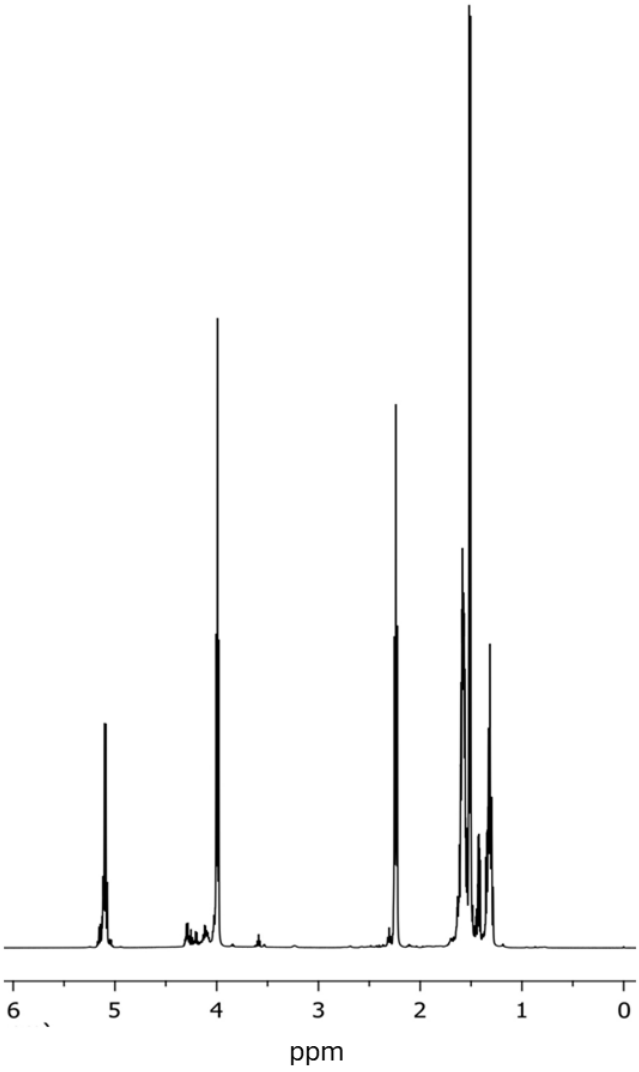

Figure 1. ^{1}H-NMR spectrum of the PLLA–PCL 2 copolymer.

The compositions in mol% of the PLLA–PCL copolymers synthesized are listed in Table 3. All copolymers are richer in PLLA. These results strongly suggest that a certain amount of PLLA end groups were not acylated during the treatment with OxCl. This means that not all PLLA chains have a terminal acyl chloride functionality. Therefore, in some PLLA chains, the hydroxyl terminal functionality remained and was able to react as the synthesis time was extended.

Table 3. Compositions in mol% of PLLA-PCL copolymers.

Copolymer	PLLA	PCL

 doi:10.20944/preprints202408.1347.v1

PLLA-PCL 1	63.0	37.0
PLLA-PCL 2	52.8	47.2
PLLA-PCL 3	62.1	37.9
PLLA-PCL 4	54.7	45.3

The ^{1}H-NMR spectrum of the PLLA–PCL–PEG 3 terpolymer is shown in Figure 2. For the PLLA–PCL–PEG terpolymers, the integral for the signal at around 3.6 ppm (after deconvolution of the end group for PCL) was used to record the amount of PEG.

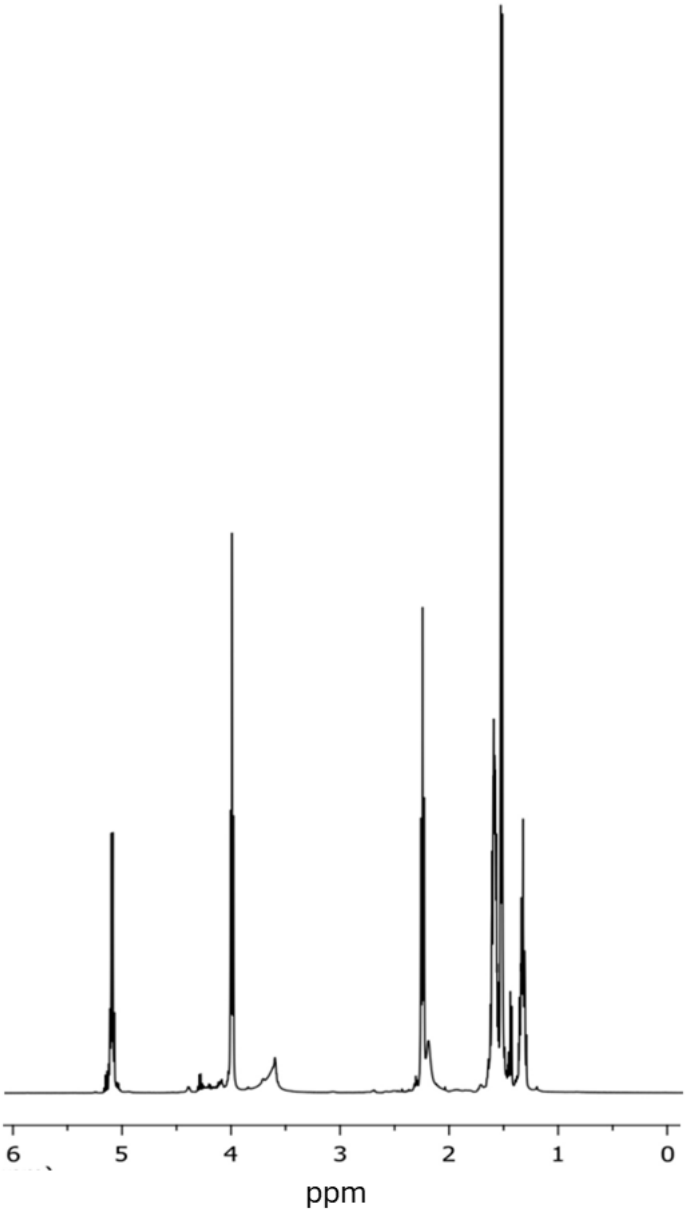

Figure 2. ^{1}H-NMR spectrum of the PLLA–PCL–PEG 3 terpolymer.

The ^{13}C-NMR spectrum of the PLLA–PCL–PEG 2 terpolymer is shown in Figure 3. The signals expected for the three repeating units (PLA, PCL, and PEG) are present. The detection of all signals indicated that the PLLA–PCL–PEG terpolymers were successfully synthesized.

Preprints.org (www.preprints.org) | NOT PEER-REVIEWED | Posted: 19 August 2024 doi:10.20944/preprints202408.1347.v1

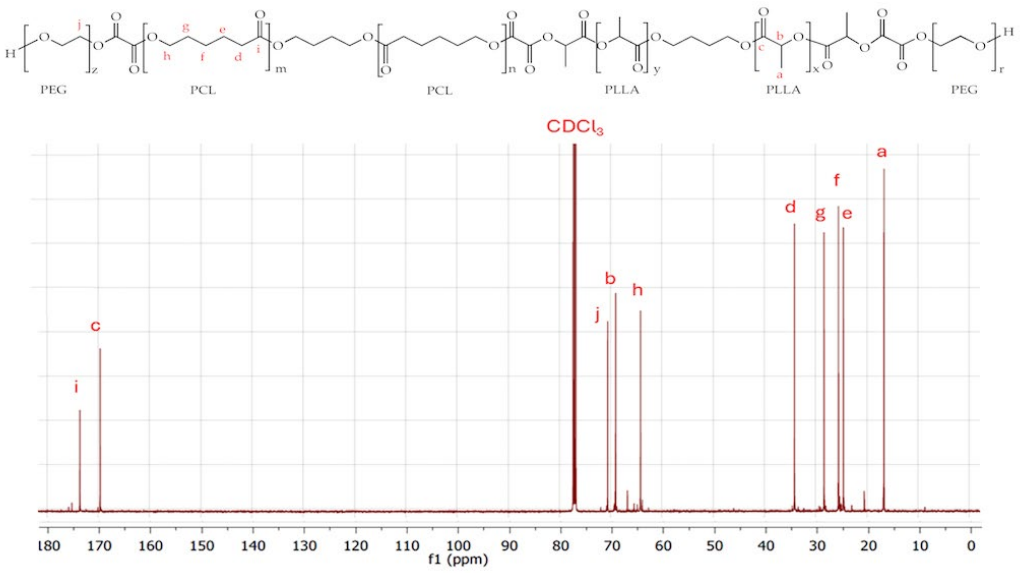

Figure 3. ^{13}C-NMR spectrum of the PLLA–PCL–PEG 2 terpolymer.

The compositions in mol% of the PLLA–PCL–PEG terpolymers are listed in Table 4. As expected, the composition of the prepared terpolymers was richer in the PLLA segments. In these PLLA–PCL–PEG terpolymers, the PEG blocks were included in low amounts (9.4–14 mol%). Nevertheless, the presence of PEG conferred a certain hydrophilic character to the hydrophobic PLLA–PCL copolymers, which was a desirable result in obtaining a nanocarrier sensitive to living matter. In this study, the PLLA–PCL–PEG 2 and PLLA–PCL–PEG 4 terpolymers are of special interest owing to their high PCL content as the hydrolysis of PCL has a strong influence on the drug release behavior of a polymer prepared with PCL.

Table 4. Compositions in mol% of PLLA-PCL-PEG terpolymers.

Terpolymer	PLLA	PCL	PEG
PLLA-PCL-PEG 1	68.2	22.4	9.4
PLLA-PCL-PEG 2	46.0	40.0	14.0
PLLA-PCL-PEG 3	51.0	38.4	10.6
PLLA-PCL-PEG 4	48.0	43.0	9.0

A series of partial IR spectra of PEG, $CNTs_{po}$, PCL 4, PLLA 1, PLLA–PCL–PEG 2, NC 2, and NC 1 presented in the region from 1500 to 1900 cm^{-1} are shown in Figure 4. The spectrum of pure PEG (Figure 4 (A)) does not present a vibrational signal in the region analyzed. Contrarily, in the spectrum of $CNTs_{po}$ (Figure 4 (B)), a wide band at 1640 cm^{-1} was detected. This band was assigned to a stretching vibration of the C=C bond conjugated to the carbonyl group. Carbonyl functionality was created on the CNT_{po} walls as a consequence of the oxidation process. Furthermore, due to this band extending until ca. 1730 cm^{-1}, also the stretching vibrations of carboxyl groups self-associated forming dimers at ca. 1700 cm^{-1} and carboxyl free groups at ca. 1720 cm^{-1}, contribute to resolve this wide band. The spectrum of PCL 4 (Figure 4 (C)) exhibited a sharp peak at 1725 cm^{-1}, which was caused by the stretching vibration of the ester carbonyl groups. For PLLA 1 (Figure 4 (D)), the stretching vibration of the carbonyl groups of ester functionality produced a wide band at 1748 cm^{-1}. In the spectrum of PLLA–PCL–PEG 2 (Figure 4 (E)), a complex and a wide band from 1650 cm^{-1} to ca. 1860 cm^{-1} was recorded. The vibrational movements of a high population of carbonyl groups were the cause of this wide band. At 1760 cm^{-1}, the most intense contribution was detected. As a weak shoulder of this band appeared another band at 1750 cm^{-1}. Subsequently, a well-resolved contribution at 1727 cm^{-1} was observed. Based on the IR spectral behavior of the pure homopolymers PCL 4 and PLLA 1 described above two assignations were made. The weak band resolved at 1750 cm^{-1} was produced by the

 doi:10.20944/preprints202408.1347.v1

stretching vibration of the ester carbonyl groups of the segments of PLLA 1, whereas the band detected at 1727 cm^{-1} was caused by the stretching vibration of the ester carbonyl groups of the segments of PCL 4. Moreover, as shown in Scheme 1, the well-known chemical reaction between the hydroxyl groups (located on the terminal chains on PLLA, PCL, and PEG blocks) and the acyl chloride groups of the OxCl was expected to occur to form the ester groups. As the vibrations of the carbonyl groups included in ester functionality resolve in the range of 1750 to 1715 cm^{-1} and the signal caused by the vibrations of dicarbonyl groups appears in the range of 1720 to 1705 cm^{-1}, it is evident that the intense band detected at 1760 cm^{-1} is originated by the vibrations of chemical groups different to ester carbonyl groups. Therefore, the band at 1760 cm^{-1} was assigned to the antisymmetric stretching vibration of the carbonyl groups of anhydride functionality. This assignation was confirmed by the fact that in the range of 1500 to 500 cm^{-1} (region not shown), the most intense band was a double band resolved at 1212 and 1191 cm^{-1}. This double band was caused by the symmetric and antisymmetric stretching vibrations of the carbonyl bonds of anhydride functionality. An anhydride functionality can be produced by the chemical reaction between the carboxyl and acyl chloride groups. Because wet BD was used in this synthesis, water moieties can act as effective alternative initiators on the homopolymerization of the PLLAs and PCLs prepared in steps 1 and 2 of the chemical procedure used in this study. A previous study reported that the homopolymerization of ε-CL initiated by water produced linear PCL chains with one carboxyl end group and one hydroxyl end group, whereas when dry BD was used as an initiator, the linear PCL synthesized contained two hydroxyl end groups [39]. Scheme 2 shows the chemical structure of the PLLA–PCL–PEG terpolymer obtained when water acts as an effective initiator of the series of PLLAs and PCLs prepared. In the IR spectra of NC 2 (Figure 4 (F)) and NC 1 (Figure 4 (G)), the spectral behavior was similar to that of the PLLA–PCL–PEG 2. Thus, in the IR spectra of both nanocomposites, three spectral contributions in 1760, 1750, and 1725 cm^{-1} were resolved. The bands detected at 1760 and 1750 cm^{-1} appeared at the same frequencies as those observed in the spectrum of PLLA–PCL–PEG 2 (Figure 4 (E)) and were caused by the vibrations of the chemical groups already described. Instead, the band detected at 1725 cm^{-1} (marked on the spectra with an arrow) was resolved to a lower frequency and at a larger intensity than the one observed in the spectrum of PLLA–PCL–PEG 2. These changes could be attributed to the formation of intermolecular hydrogen bonds created between the carboxyl groups inserted on the walls of $CNTs_{po}$ and the carbonyl groups of ester functionality of the PCL chains. The formation of hydrogen bonds in nanocomposites prepared with CNTs functionalized with carboxyl groups and a polymer containing carbonyl groups has been previously reported [40,41].

 doi:10.20944/preprints202408.1347.v1

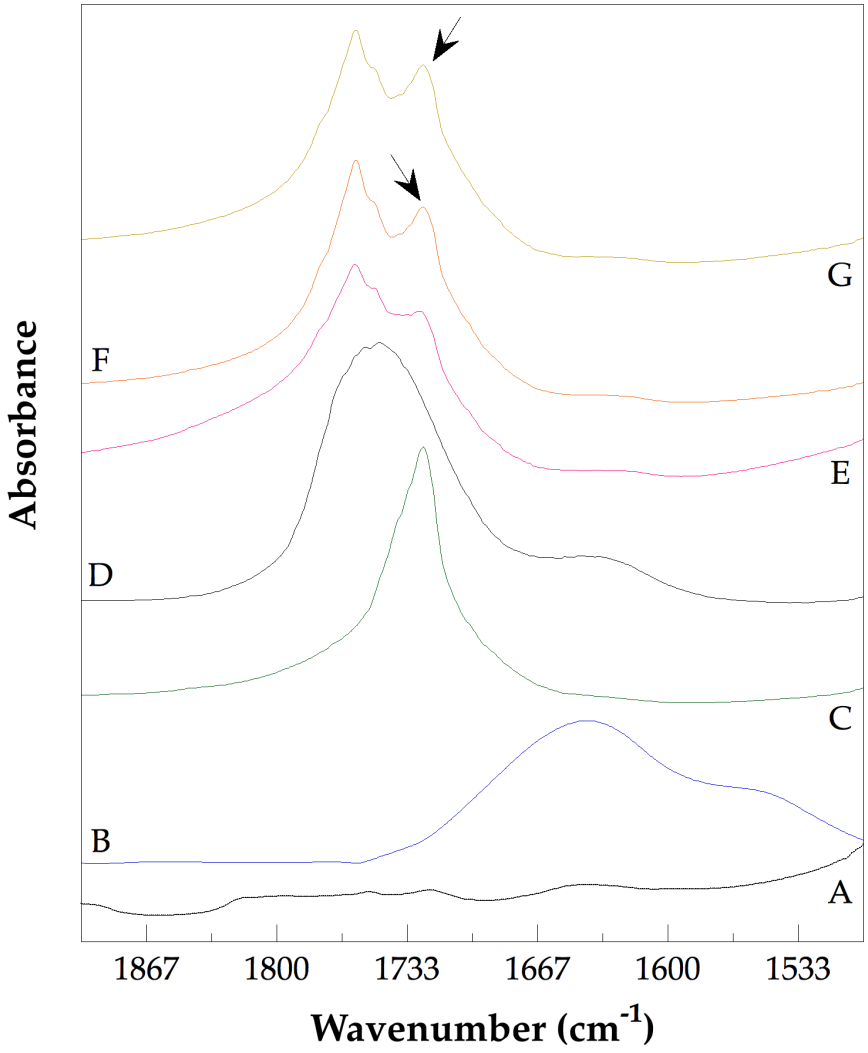

Figure 4. Partial IR spectra centered in the 1500 to 1900 cm^{-1} region of PEG (A), $CNTs_{po}$ (B), PCL 4 (C), PLLA 1 (D), PLLA–PCL–PEG 2 (E), NC 2 (F), and NC 1 (G).

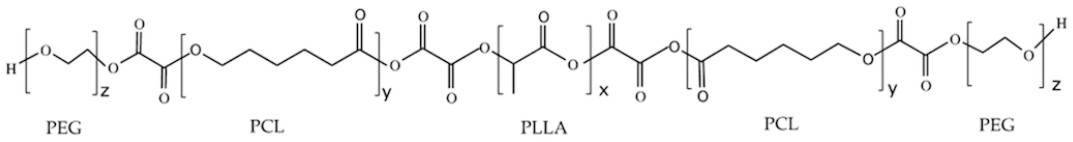

Scheme 2. Chemical structure of the prepared PLLA-PCL-PEG terpolymers when water acts as an effective initiator.

Figure 5 shows the partial spectra of $CNTs_{po}$, PCL 4, PLLA 1, PEG, PLLA–PCL–PEG 2, NC 2, and NC 1 centered in the 3050 to 3900 cm^{-1} region. In the spectrum of $CNTs_{po}$ (Figure 5 (A)), a broad band at 3527 cm^{-1} due to the stretching vibration of the hydroxyl groups was detected. A similar broad band assigned to the stretching vibration of the hydroxyl groups on the FT-IR spectrum of a sample of multiwalled carbon nanotubes (MWCNTs) has been reported elsewhere [42]. In the spectrum of PCL 4 (Figure 5 (B)), a broad band with two peaks was detected. The first peak was sharp and was detected at 3438 cm^{-1}, whereas the second peak was wide and appeared at 3536 cm^{-1}. This broad band was due to the stretching vibration of the hydroxyl groups. For polymers that contain

 doi:10.20944/preprints202408.1347.v1

hydroxyl and carbonyl groups, the summation of the vibrations of several chemical bonds produces this band. From the lower to the higher frequencies, vibrations of different types of hydroxyl groups occurred: (i) self-associated hydroxyl groups forming dimers, trimers, etc., (ii) hydrogen bonded to the carbonyl groups, and (iii) free [43]. The vibrations of the free hydroxyl groups produced weak and sharp bands above 3615 cm^{-1} [44]. Therefore, we considered that the peak at 3438 cm^{-1} was caused by hydroxyl–hydroxyl self-associated movements, whereas the peak at 3536 cm^{-1} was due to hydroxyl–carbonyl vibrations. Concerning the PLLA 1 and PEG homopolymers, it is evident that their vibrational behaviors are similar. In the spectrum of PLLA (Figure 5 (C)), only one band at 3479 cm^{-1} was detected, whereas in the spectrum of PEG (Figure 5 (D)), also one band at 3470 cm^{-1} was observed. Both spectral contributions were assigned to the stretching vibration of the hydroxyl groups. Contrarily, in the spectrum of PLLA–PCL–PEG 2 (Figure 5 (E)), three spectral contributions were detected. At 3649 cm^{-1}, a weak sharp band assigned to vibrations of the free hydroxyl groups appeared. Moreover, a broad band at 3500 cm^{-1} with a shoulder at 3460 cm^{-1} was detected. The stretching vibration of the hydroxyl groups produced this broad band. In the spectra of NC 2 (Figure 5 (F)) and NC 1 (Figure 5 (G)), three bands were also detected. However, now the band due to vibrations of free hydroxyl groups (indicated by an arrow) was detected to lower frequencies and appeared in both spectra at 3637 cm^{-1}, whereas the stretching vibration of the hydroxyl groups produced the broad band at 3502 cm^{-1} with a shoulder at 3436 cm^{-1} (indicated by an arrow) (Figure 5 (F)) and at 3437 cm^{-1} (indicated by an arrow) (Figure 5 (G)). The fact that this shoulder appeared at a lower frequency compared with the band detected at 3438 cm^{-1} in the spectrum of PCL 4 suggests that hydrogen bonds formed between the ester carbonyl groups of PCL 4 and the hydroxyl groups of the $CNTs_{po}$ inserted in NC 2 and NC 1. These results along with the results obtained from the analysis of the spectra shown in Figures 4 (E), (F), and (G) suggest that the $CNTs_{po}$ develops a preferential orientation to PCL 4 blocks.

 doi:10.20944/preprints202408.1347.v1

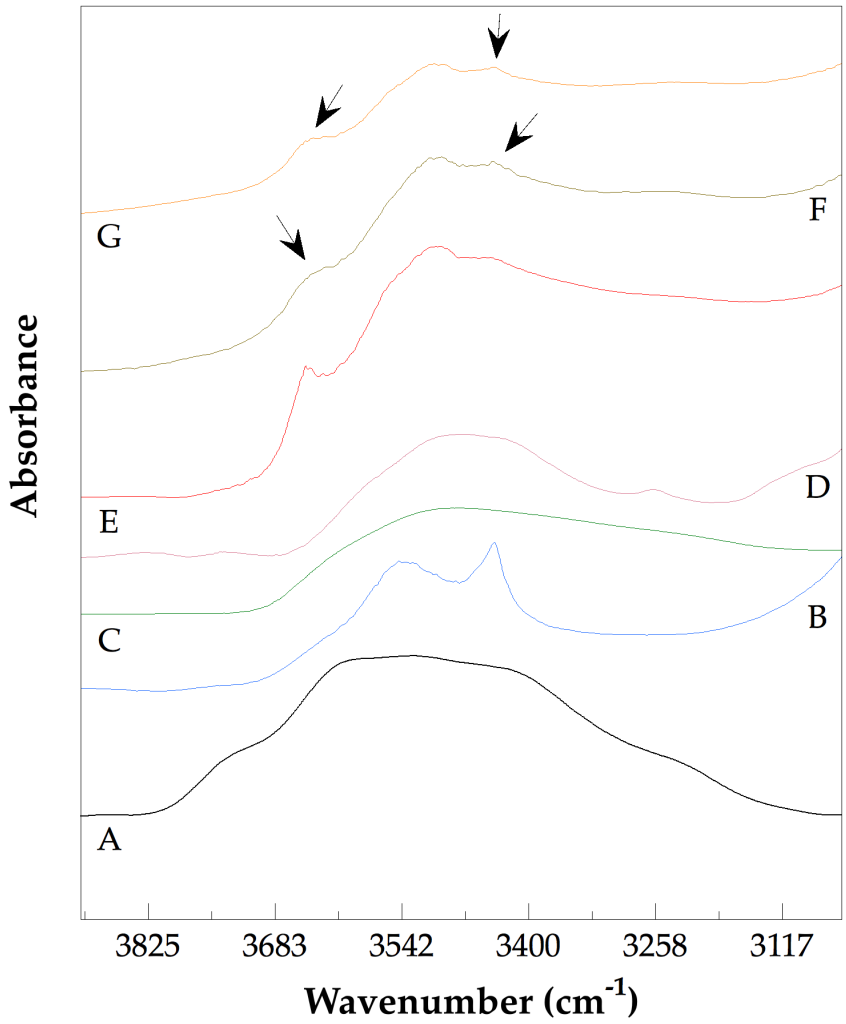

Figure 5. Partial IR spectra delimited on the 3050 to 3900 cm^{-1} region of $CNTs_{po}$ (A), PCL 4 (B), PLLA 1 (C), PEG (D), PLLA–PCL–PEG 2 (E), NC 2 (F), and NC 1 (G).

The *C1s* core level normalized spectra of the PLLA–PCL–PEG 4 terpolymer and NC 4 and NC 3 are presented in Figure 6. The active background approach encompassed in the Analyzer v 1.33 software was used to make the peaks fit [45]. The spectra were adjusted using the respective shift according to the C–C bond position at 285.0 eV. The *C1s* core level normalized spectrum of the PLLA–PCL–PEG 4 terpolymer (Figure 6 (A)) shows components at four positions, which are at 285.0 eV (C–C/C–H bonds) [46], 286.2 eV (C–O–C groups of PEG/–(C=O)–O–CH_2–functionality of PCL) [47], 287.1 eV (–CH–(CH_3)–(C=O)–O– functionality of PLLA) [47], and 289.1 eV ((–CH–(CH_3)–(C=O)–O– functionality of the PLLA/–CH_2–(C=O)–O–) groups of PCL) [47]. The calculated atomic concentrations of the mentioned groups were 36.4%, 14.7%, 7.8%, and 12.7%, respectively. In the *C1s* core level normalized spectra of NC 4 and NC 3, components at four positions were also detected. The components and their calculated atomic concentrations detected in the spectrum of NC 4 (Figure 6 (B)) were 285.0 eV (C–C/C–H bonds) [46] 46.0%, 286.3 eV (C–O–C groups of PEG/–(C=O)–O–CH_2–functionality of PCL) [47] 9.1%, 287.0 eV (–CH–(CH_3)–(C=O)–O– functionality of PLLA) [47] 6.8%, and 289.1 eV ((–CH–(CH_3)–(C=O)–O–functionality of PLLA/–CH_2–(C=O)–O–) groups of PCL) [47] 12.6%. In a similar form by analysis of the spectrum of NC 3 (Figure 6 (C)), the results were 285.0 eV (C–C/C–H bonds) [46] 59.7%, 286.3 eV (C–O–C groups of PEG/–(C=O)–O–CH_2–functionality of PCL) [47] 11.4%, 287.0 eV (–CH–(CH_3)–(C=O)–O– functionality of PLLA) [47] 7.8%, and 289.1 eV ((–CH–(CH_3)–(C=O)–O–functionality of PLLA/–CH_2–(C=O)–O–) groups of PCL) [47] 14.9%. As previously reported, ester groups are sensitive to develop a reaction of nucleophilic substitution [48]. The PLLA–PCL–PEG terpolymers are rich in ester groups. The nanocomposites were prepared in an aprotic

 doi:10.20944/preprints202408.1347.v1

solvent (THF). On the walls of the $CNTs_{po}$ there are hydroxyl groups. The hydroxyl group is nucleophilic and highly reactive. Moreover, in the chemical structure of the PLLA–PCL–PEG terpolymers, dicarbonyl groups exist. Because of the higher reactivity of the dicarbonyl groups than the carbonyl groups, it is possible that they are more sensitive to a chemical attack from the hydroxyl groups of the $CNTs_{po}$. The fact of the concentration molar of ester groups of the NC 3 and NC 4 decreases (also detected in the *O1s* core level normalized spectra of both nanocomposites (not shown)) respect to the observed in the spectrum of the PLLA–PCL–PEG 4, strongly suggests that a nucleophilic substitution reaction was performed. This implies that the chains of the PLLA–PCL–PEG 4 are grafted to the walls of the $CNTs_{po}$. Scheme 3 shows the aforementioned chemical reaction, in which the nucleophilic substitution on a carbonyl group of the dicarbonyl functionality is exemplified.

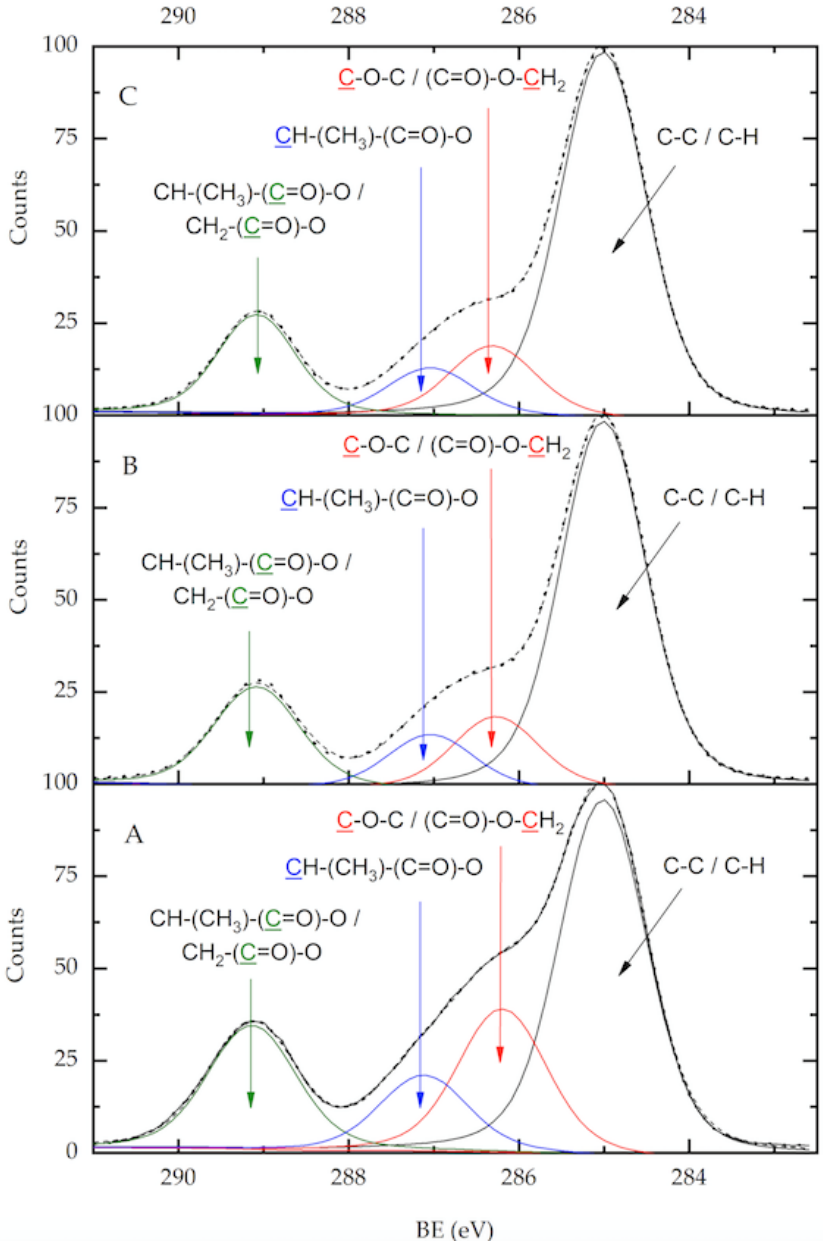

Figure 6. *C1s* core level normalized spectra of PLLA–PCL–PEG 4 (A), NC 4 (B), and NC 3 (C).

 doi:10.20944/preprints202408.1347.v1

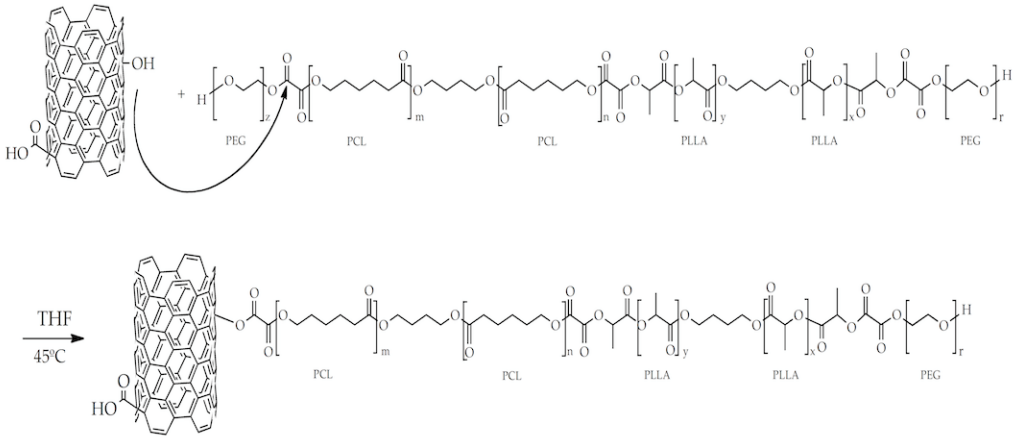

Scheme 3. Grafting chemical reaction for preparing the PLLA-PCL-PEG/CNTs$_{po}$ nanocomposites.

3.4. Thermal Analysis of the PLLA–PCL–PEG Terpolymers and of the PLLA–PCL–PEG/CNT$_{po}$ Nanocomposites

Figure 7 presents the DSC thermograms of PLLA–PCL–PEG 4, NC 3, and NC 4. The DSC results obtained from the analysis of the thermograms of PLLA–PCL–PEG 2, PLLA–PCL–PEG 4, NC 1, NC 2, NC 3, and NC 4 are summarized in Table 5. Supplementary material shows the DSC thermograms of the homopolymers PEG, PCL 4, and PLLA 4. The DSC thermal behavior of the pure homopolymers is described below. Thus, in the DSC thermogram of PEG, a glass transition relaxation (T_{gPEG} = −13°C (260.15K)) and a melting endotherm (T_{mPEG} = 61.0°C (334.15 K), ΔH_{mPEG} = 60.8 J/g) were detected. In the DSC thermogram of PCL 4, a glass transition temperature ($T_{gPCL\,4}$ = −59°C (214.15 K)) and a melting endotherm ($T_{mPCL\,4}$ = 55.0°C (328.15 K), $\Delta H_{m\,PCL\,4}$ = 77.7 J/g) were detected. Furthermore, in the DSC thermogram of PLLA 1, a glass transition temperature ($T_{gPLLA\,1}$ = 50°C (323.15 K)), a crystallization exotherm ($T_{cPLLA\,1}$ = 111.6°C (384.75 K), $\Delta H_{cPLLA\,1}$ = 49.1 J/g), and a melting endotherm ($T_{mPLLA\,1}$ = 151.4°C (424.55 K), $\Delta H_{mPLLA\,1}$ = 42.6 J/g) were observed. Based on these results, the DSC thermogram of the PLLA–PCL–PEG 4 terpolymer was analyzed. In the DSC thermogram of PLLA–PCL–PEG 4 (Figure 7 (A)), two glass transition relaxations and two melting endotherms were detected. T_{g1} = −50°C (223.15 K) was assigned to the relaxations in the amorphous phase of the PCL 4 chains, whereas T_{g2} = 14°C (287.15 K) was assigned to domains rich in PEG chains. These thermal relaxations were detected at a higher temperature than those recorded in the thermograms of the pure homopolymers of PCL 4 and PEG, indicating that the crystalline phases detected in the thermogram of the terpolymer limited the relaxations in the amorphous phase. The first melting endotherm was resolved in a range of temperatures from 35°C (308.15 K) to 55°C (328.15 K) and exhibited two peaks. In this temperature range, relaxation in the amorphous phase of PLLA 1 chains, melting of the PCL 4 chains, and melting of the PEG chains occurred. The first peak T_{m1} = 44.3°C (317.45 K) is intense, while the second peak T_{m2} = 50.4°C (323.55 K) is weak. When a melted block copolymer is quenched below the melting temperature, the microphase separation and the crystallization occur, simultaneously. Competition in the crystallization of the blocks is developed. Several studies focus on the melting behavior of the PCL–PEG diblock copolymer. A study about PCL–PEG diblock copolymers with M_n = 20,000–30,000 prepared with PCL weight fractions ranging from 68% to 85% concluded that PCL blocks crystallize first, which induces an imperfect crystallization of PEG blocks [49,50]. Another study on the crystallization of PCL–PEG diblock copolymers synthesized with a PCL weight fraction of 34% to 67% concluded that PCL chains crystallize first. After this, crystallization of PEG chains occurred [51]. Xu et al. studied the crystallization of PCL–PEG copolymers with $M_{n,PEG}$ = 5000 and concluded that PCL blocks disfavor the crystallization of PEG blocks and vice versa [52]. This explains the small value of ΔH_{m1} (shown in Table 5) for both PLLA–PCL–PEG 4 and PLLA–PCL–PEG 2. Furthermore, in another study of PEG–PCL diblock copolymer prepared with PEG (M_n = 5000) and PCL (M_n =

 doi:10.20944/preprints202408.1347.v1

9200), two melting peaks were observed in the melting endotherm detected through DSC, which were assigned to the melting of the PEG (first peak) domains and the melting of the PCL (second peak) domains. XRD measurements support this analysis [53]. Similar results were recorded in a study of segmented PCL/PEG–based poly(urethane urea) copolymers prepared with PCL/PEG weight ratio = 80/20 and M_w = 67000. On the melting endotherm, two melting peaks were detected. The first peak was caused by the melting of the PEG domains and the second peak by the melting of the PCL domains [54]. Therefore, it is reasonable to consider that in the DSC endotherm of PLLA–PCL–PEG 4, the first peak (T_{m1} = 44.3°C (317.45 K)) was caused by the melting of the PEG domains and the second peak (T_{m2} = 50.4°C (323.55 K)) is due the melting of the PCL 4 domains. In some cases, in the endotherm of the PCL–PEG copolymers, only one T_m has been detected, as reported elsewhere [55]. As shown in Table 5, for PLLA–PCL–PEG 2, only one melting temperature (T_{m1} = 44.3°C (317.45 K)) was detected, indicating the simultaneous crystallization of PCL and PEG blocks. Additionally, the second endotherm of the DSC thermogram of the PLLA–PCL–PEG 4 terpolymer was detected in a range of temperatures from ca. 100°C (373.15 K) to 135°C (408.15 K), in which T_{m3} = 125.4°C (398.55 K) was detected, and was due to the melting of the PLLA 1 domains. Evidently, this melting temperature was detected to lower temperature than the melting temperature of the pure PLLA 1. This means that the complex morphology of the PLLA–PCL–PEG 4 terpolymer has a strong influence on the melting of the PLLA 1 domains.

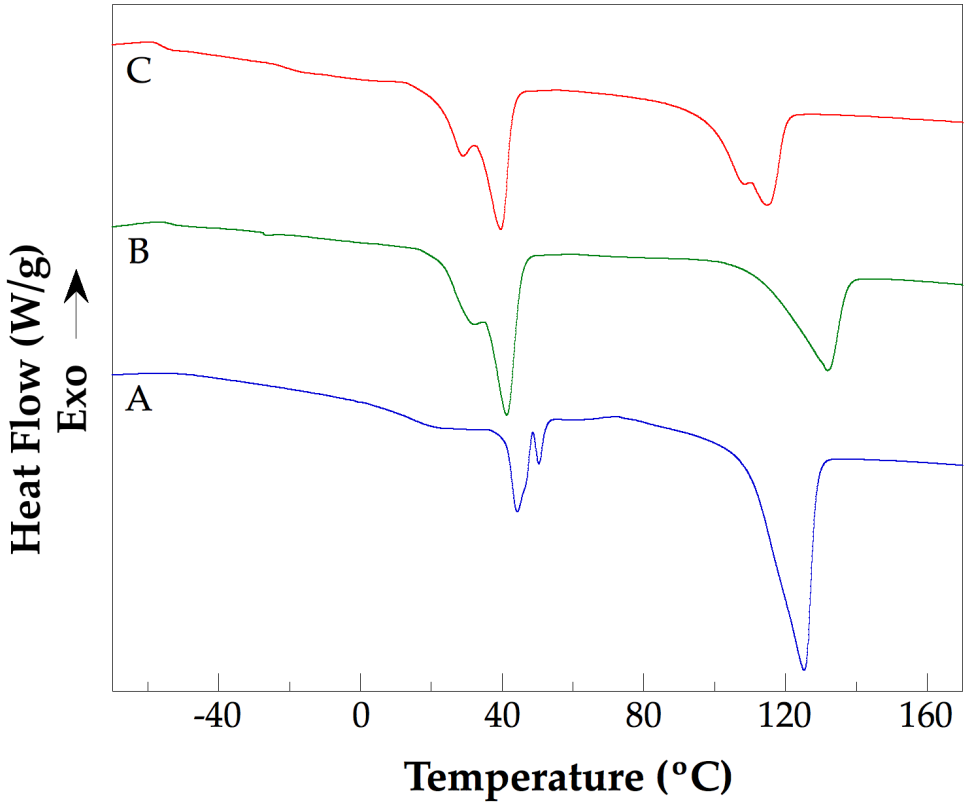

Figure 7. DSC thermograms of PLLA–PCL–PEG 4 (A), NC 3 (B), and NC 4 (C).

Table 5. Results of the analysis of the DSC thermograms of the PLLA-PCL-PEG terpolymers and PLLA-PCL-PEG/CNTs$_{po}$ nanocomposites used in the tests of the methotrexate release.

Sample	T_{g1} (K)	T_{g2} (K)	T_{m1} (K)	T_{m2} (K)	ΔH_{m1} J/g	T_{m3} (K)	ΔH_{m2} J/g
PLLA-PCL-PEG 2	221.15	287.15	318.45	-	8.1	398.85	35.9
PLLA-PCL-PEG 4	223.15	285.15	317.45	323.55	8.0	398.55	36.6

 doi:10.20944/preprints202408.1347.v1

NC 1	216.15	291.15	313.95	319.85	30.2	413.65	29.6
NC 2	218.15	258.15	312.65	319.45	33.6	413.35	28.5
NC 3	219.15	290.15	305.55	314.45	26.4	405.05	19.9
NC 4	217.15	252.15	302.15	312.75	23.3	387.95	20.5

As regards the thermal behavior of the nanocomposites, although two glass transition relaxations and two melting endotherms were observed in their DSC thermograms (Figure 7 (B) for NC 3 and Figure 7 (C) for NC 4), significant changes were detected compared to the observed in the thermograms of their pure polymer matrices. Thus, (i) for all nanocomposites, T_{g1} due to the glass transition of the PCL 4 chains was detected at lower temperatures than that observed for their pure polymeric matrix; (ii) for NC 2 and NC 4 (both prepared with 0.5 wt.% $CNTs_{po}$), T_{g2} caused by the glass transition relaxation of the PEG chains was detected at a lower temperature than that of PEG pure. Contrarily, for NC 1 and NC 3 (both prepared with 1.0 wt.% $CNTs_{po}$), T_{g2} was detected at a higher temperature. The increase of the value of glass transition temperature of nanocomposites prepared with CNTs has been explained as a consequence of the reduction in the mobility of the polymer chains. This reduction is induced for the physical and chemical interacctions formed between the chemical groups inserted on the walls of the $CNTs_{po}$ and the chemical groups of the polymer chains of the polymeric matrices of the studied nanocomposites. Similar results for the nanocomposites of PMMA and amino-functionalized CNTs have been reported elsewhere [56]. Our results indicate that the reduction in the mobility of polymer chains depends on the amount of $CNTs_{po}$ used in the preparation of the studied nanocomposites. Contrarily, the decrease in the glass transition temperature has been explained as a consequence of the high dispersion of CNTs and the formation of a thin film of nanoscale confined polymer between CNTs, as was reported in a study of nanocomposites prepared with polycarbonate (as polymer matrix) and functionalized MWCNTs previously published [57]. The small amount of $CNTs_{po}$ used to prepare the NC 2 and NC 4 favors to obtain a high dispersion of $CNTs_{po}$. Moreover, the presence of $CNTs_{po}$ in the studied nanocomposites has a different influence on the melting of domains rich in PEG/PCL 4 chains or domains rich in PLLA 1 chains. Thus, a clear change is observed in the first endotherm of the DSC thermograms of all the prepared nanocomposites. A difference to the recorded in the DSC thermogram of the PLLA–PCL–PEG 4 terpolymer, in which the most intense peak was the first, and corresponds to the melting of PEG chains, for the nanocomposites NC 3 and NC 4, the peak most intense is the second. This second peak is produced by the melting of the PCL chains. Furthermore, the ΔH_{m1} of all the nanocomposites is larger than those of their polymer matrices (PLLA–PCL–PEG 2 and PLLA–PCL–PEG 4). These results indicate that $CNTs_{po}$ act as nucleation sites of the PCL 4 chains. The role of CNTs (functionalized with the hydroxyl and carboxyl groups) as nucleating agents in nanocomposites prepared with a semicrystalline polymer has been previously reported [58]. Contrarily, for the second endotherm, the ΔH_{m2} (associated with the melting of PLLA 1 chains) of all the nanocomposites decreased compared to the second endotherm observed in the DSC thermograms of the pure polymer matrices. In this case, $CNTs_{po}$ act as antinucleating agents. The thermal behavior related to the melting of the prepared nanocomposites strongly suggests that the $CNTs_{po}$ preferentially are oriented to the PCL 4 chains.

3.5. Analysis of Methotrexate In Vitro Release Profiles from PLLA–PCL–PEG Terpolymers and of the PLLA–PCL–PEG/CNT_{po} Nanocomposites

Figure 8 presents the methotrexate in vitro release patterns for the PLLA–PCL–PEG 2 terpolymer and NC 1 and NC 2, whereas Figure 9 shows the release profiles for the PLLA–PCL–PEG 4 terpolymer and NC 3 and NC 4. In both figures, the error bars of all the recovered data are included. An inset was included, in which the methotrexate release data recorded until 4 h are shown. During the release test, the tablets of the terpolymers and the nanocomposites were eroded. Such an erosion was faster for the PLLA–PCL–PEG 2 and PLLA–PCL–PEG 4 terpolymers than for the nanocomposites prepared with them. Moreover, the release from the terpolymers was faster than that from the nanocomposites. Thereby, the methotrexate release rates from PLLA–PCL–PEG 2 and PLLA–PCL–PEG 4 were 44.1%

 doi:10.20944/preprints202408.1347.v1

and 60.4% at 12 h, respectively. The highest release was obtained at 54 h for PLLA–PCL–PEG 2 (99.5%) and at 48 h for PLLA–PCL–PEG 4 (98.8%). Contrarily, the methotrexate release rates for NC 1, NC 2, NC 3, and NC 4 were 41.8%, 41.0%, 38.8%, and 43.1% at 12 h, respectively. Moreover, the highest release rates for NC 1, NC 2, NC 3, and NC 4 were 98.7%, 98.5%, 98.0%, and 98.8% at 96 h, respectively. Evidently, the release evolution of all the studied terpolymers and nanocomposites follow a biphasic cumulative release behavior characterized by a "burst release" at the initial times and a plateau ("power-law phase"), which is smaller for PLLA–PCL–PEG 2 and PLLA–PCL–PEG 4 than for the nanocomposites. The "burst release" for the nanocomposites in the first moments was attenuated, as can be observed in the insets of Figures 8 and 9. This effect was more evident for NC 3 and NC 4, which were prepared with a polymer matrix of PLLA–PCL–PEG 4. The fact that this terpolymer has a lower content of PEG than the PLLA–PCL–PEG 2 terpolymer indicates that it is more hydrophobic, which, combined with the presence of $CNTs_{po}$, favors a slower methotrexate release.

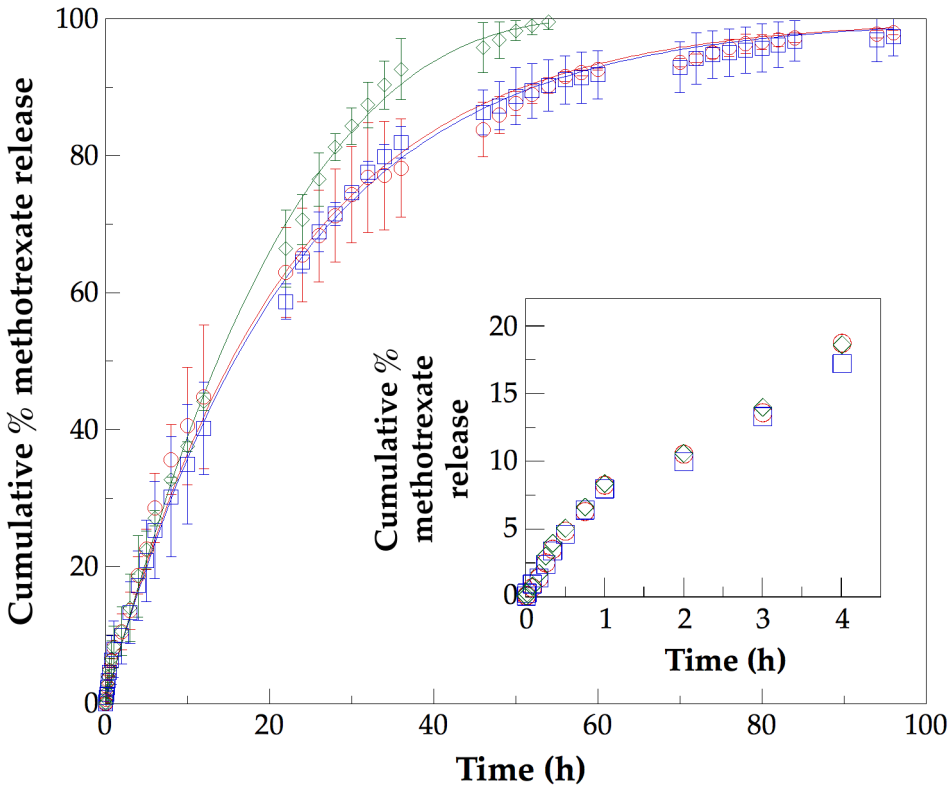

Figure 8. Methotrexate in vitro release profiles for PLLA–PCL–PEG 2 (◊), NC 1 (○), and NC 2 (□). As inset, the methotrexate release data without error bars until 4 h were included.

 doi:10.20944/preprints202408.1347.v1

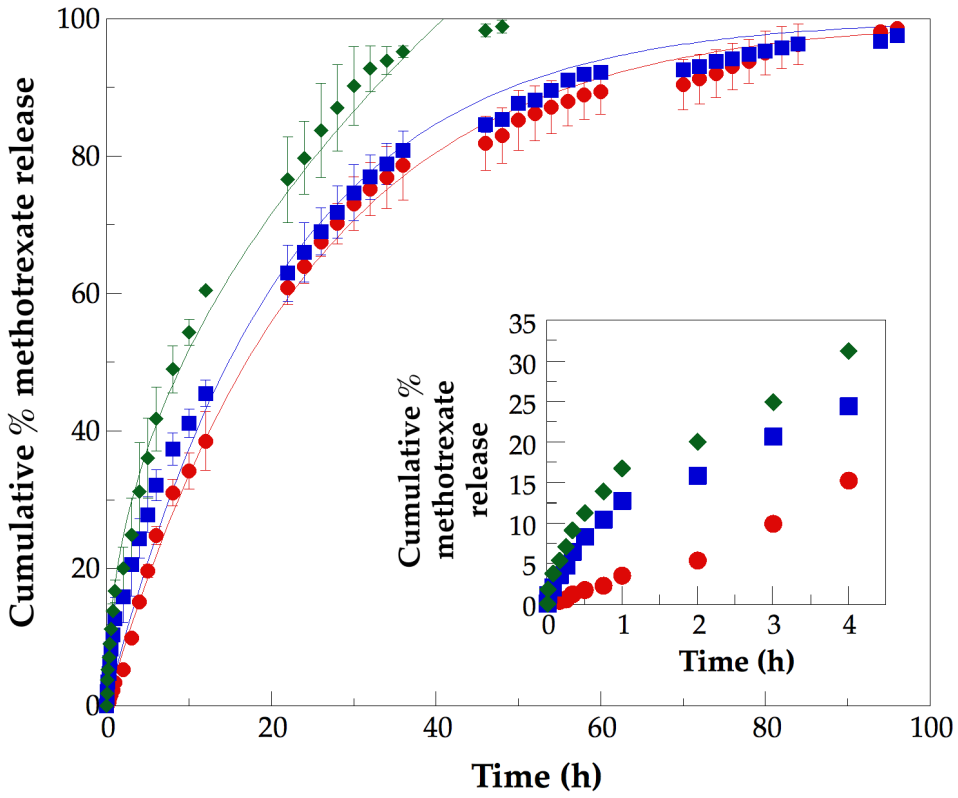

Figure 9. Methotrexate in vitro release patterns for PLLA–PCL–PEG 4 (♦), NC 3 (●), and NC 4 (■). An inset shows the methotrexate release data without error bars until 4 h.

Five models were used to fit the methotrexate release data. These models were Higuchi (1), Korsmeyer–Peppas (2), Korsmeyer–Peppas extended (3), first order (4), and Hixson–Crowell (5). In all cases, F denotes the percentage of drug released, which is determined from M_t/M_∞, the fraction of drug release at time t, where M_t denotes the amount of drug released at time t, and M_∞ denotes the amount of drug loaded:

$$F = k_H\, t^{\frac{1}{2}} \quad (1)$$

where k_H denotes the kinetic rate constant of the Higuchi model, which depends on the variables of the release system, and t denotes the time. Higuchi's model is based on Fick's second law [59].

$$F = k_{KP}\, t^n \quad (2)$$

where k_{KP} denotes the kinetic rate constant of the Korsmeyer–Peppas model and n is the release exponent. This exponent characterizes the release mechanism from polymer matrices, which can have different geometries. The Korsmeyer–Peppas model was proposed to assess the released drugs from a polymer matrix [60].

$$F = k'_{KP}\, t^n + b \quad (3)$$

where k'_{KP} denotes the kinetic rate constant of the Korsmeyer–Peppas extended model and b denotes the "burst effect." This model is an extension of the Korsmeyer–Peppas model and was proposed to evaluate the "burst effect" [61].

$$F = 100\,(1 - e^{-k_1\, t}) \quad (4)$$

where k_1 denotes the first-order release constant [62]. Using Fick's first law is possible obtain a relationship among k_1 and the diffusion constant in the release medium. A wide variety of systems follow this model.

$$F = 100\,[1 - (1 - k_{HC}\, t)^3] \quad (5)$$

where k_{HC} denotes the release constant of the Hixson–Crowell model [63]. This model applies to tablets and considers the dissolution carried out in planes parallel to the surface of the tablet.

To fit the experimental data to the drug release kinetic models, the DDSolver software was used [64]. Among the statistical criteria provided by DDSolver to evaluate the goodness of fit of a model,

 doi:10.20944/preprints202408.1347.v1

the coefficient of determination (R^2), mean square error (MSE), and model selection criterion (MSC) were used in this study. In the comparison of different models, the most appropriate model is the one with the largest MSC. A good fit is achieved when an MSC value larger than 2 or 3 is determined [65]. Table 6 shows the kinetic parameters for methotrexate release from tablets of PLLA-PCL-PEG 2 terpolymer and NC 1 and NC 2 nanocomposites. In contrast, Table 7 presents the kinetic parameters obtained for release tests realized with tablets of PLLA-PCL-PEG 4 terpolymer and NC 3 and NC 4 nanocomposites.

Table 6. Kinetic parameters for methotrexate release from tablets of PLLA-PCL-PEG 2 terpolymer, and NC 1, and NC 2 nanocomposites determined with Higuchi, Korsmeyer-Peppas, Korsmeyer-Peppas extended, First order, and Hixson-Crowell models.

Models		Tested Materials		
		PLLA-PCL-PEG 2	NC 1	NC 2
Higuchi	$k_H\ \left(h^{-\frac{1}{2}}\right)$	14.12 ± 0.36	11.56 ± 0.29	11.51 ± 0.24
	R^2	0.975 ± 0.013	0.963 ± 0.024	0.960 ± 0.002
	MSE	39.95 ± 23.93	53.16 ± 33.81	59.26 ± 6.58
	MSC	3.67 ± 0.54	3.31 ± 0.70	3.11 ± 0.05
Korsmeyer-Peppas	$k_{KP}\ (h^{-n})$	10.34 ± 0.71	14.87 ± 3.61	14.18 ± 2.89
	n	0.59 ± 0.03	0.44 ± 0.05	0.45 ± 0.06
	R^2	0.984 ± 0.008	0.972 ± 0.012	0.966 ± 0.008
	MSE	26.57 ± 16.16	41.72 ± 17.77	51.47 ± 19.53
	MSC	4.02 ± 0.53	3.46 ± 0.46	3.26 ± 0.23
Korsmeyer-Peppas extended[1]	$k'_{KP}\ (h^{-n})$	6.92 ± 3.69	6.64 ± 0.49	6.47 ± 3.36
	n	0.77 ± 0.24	0.78 ± 0.05	0.76 ± 0.14
	b	0.12 ± 0.69	0.12 ± 0.37	0.12 ± 0.17
	R^2	0.995 ± 0.003	0.993 ± 0.004	0.996 ± 0.002
	MSE	1.19 ± 0.85	1.68 ± 0.23	0.88 ± 0.73
	MSC	4.99 ± 0.70	4.60 ± 0.54	5.17 ± 0.55
First order	$k_1(h^{-1})$	0.06 ± 0.003	0.05 ± 0.008	0.04 ± 0.001
	R^2	0.991 ± 0.001	0.996 ± 0.003	0.993 ± 0.005
	MSE	13.88 ± 3.78	5.85 ± 3.91	10.01 ± 5.32
	MSC	4.61 ± 0.16	5.53 ± 0.74	4.96 ± 0.72
Hixson-Crowell	$k_{HC}\ \left(h^{-\frac{1}{3}}\right)$	0.015 ± 0.001	0.012 ± 0.002	0.012 ± 0.001
	R^2	0.995 ± 0.004	0.985 ± 0.010	0.983 ± 0.020
	MSE	6.47 ± 5.28	21.18 ± 13.68	21.60 ± 25.91
	MSC	5.56 ± 1.04	4.23 ± 0.71	4.75 ± 1.93

[1] To make the determination of burst affect was analyzed the portion of release curve where $F < 44.8\%$.

Table 7. Kinetic parameters for methotrexate release from tablets of PLLA-PCL-PEG 4 terpolymer, and NC 3, and NC 4 nanocomposites determined with Higuchi, Korsmeyer-Peppas, Korsmeyer-Peppas extended, First order, and Hixson-Crowell models.

Models		Tested Materials		
		PLLA-PCL-PEG 4	NC 3	NC 4
Higuchi	$k_H\ \left(h^{-\frac{1}{2}}\right)$	15.86 ± 0.35	11.26 ± 0.38	11.56 ± 0.17
	R^2	0.985 ± 0.002	0.966 ± 0.006	0.961 ± 0.015
	MSE	19.58 ± 4.40	50.50 ± 13.51	51.48 ± 17.69
	MSC	4.10 ± 0.11	3.29 ± 0.18	3.16 ± 0.38
Korsmeyer-Peppas	$k_{KP}\ (h^{-n})$	17.65 ± 1.93	12.71 ± 0.14	17.20 ± 2.33
	n	0.47 ± 0.04	0.47 ± 0.01	0.40 ± 0.03

 doi:10.20944/preprints202408.1347.v1

	R^2	0.989 ± 0.006	0.967 ± 0.007	0.979 ± 0.002
	MSE	16.33 ± 10.25	49.82 ± 14.44	28.39 ± 2.04
	MSC	4.34 ± 0.56	3.28 ± 0.20	3.70 ± 0.10
Korsmeyer-Peppas extended[1]	k'_{KP} (h^{-n})	13.75 ± 5.67	4.88 ± 0.33	11.83 ± 3.21
	n	0.61 ± 0.14	0.86 ± 0.06	0.56 ± 0.09
	b	0.89 ± 2.83	- 0.86 ± 0.18	- 0.38 ± 0.51
	R^2	0.993 ± 0.005	0.988 ± 0.003	0.997 ± 0.001
	MSE	2.66 ± 1.66	2.43 ± 0.15	0.65 ± 0.11
	MSC	4.76 ± 0.79	4.05 ± 0.23	5.54 ± 0.23
First order	$k_1(h^{-1})$	0.08 ± 0.001	0.04 ± 0.004	0.05 ± 0.005
	R^2	0.981 ± 0.015	0.996 ± 0.003	0.987 ± 0.006
	MSE	25.01 ± 17.65	5.55 ± 3.84	16.28 ± 7.78
	MSC	3.98 ± 0.89	5.61 ± 0.85	4.34 ± 0.53
Hixson-Crowell	k_{HC} $\left(h^{-\frac{1}{3}}\right)$	0.02 ± 0.001	0.01 ± 0.001	0.01 ± 0.001
	R^2	0.964 ± 0.032	0.984 ± 0.011	0.970 ± 0.010
	MSE	46.05 ± 37.69	21.98 ± 14.72	39.53 ± 11.87
	MSC	3.43 ± 1.05	4.23 ± 0.82	3.41 ± 0.34

[1] The burst effect was evaluated by analysis the portion of release curve in which F < 60.5%.

For NC 1, NC 2, NC 3, and NC 4, a comparison of the results shown in Tables 6 and 7 indicates that the first-order model fit the experimental data with the best accuracy. This statement is based on the fact that in general, it was fulfilled that the R^2 values are close to the unity, the MSE values are minimal, and the MSC values are maximum. Contrarily, taking into count these three criteria, for the PLLA–PCL–PEG 2 and PLLA–PCL–PEG 4 terpolymers, the best models were Hixson–Crowell and Korsmeyer–Peppas, respectively. In Figures 8 and 9, the solid lines traced over the experimental data of each type of the nanocomposite or terpolymer correspond to the fit of the best model mentioned above.

It is important to analyze the result obtained from the Korsmeyer–Peppas model as its exponent n provides information regarding the drug release mechanism. The values of n for the nanocomposites were 0.44 (NC 1), 0.45 (NC 2), 0.47 (NC 3), and 0.40 (NC 4). Therefore, the Fickian diffusion drives the methotrexate release, specifically for a planar (thin films) matrix (NC 3), cylinder-shaped matrix (NC 1 and NC 2), and sphere-shaped matrix (NC 4). For the last nanocomposite (NC 4), the value of n was minor than the typical value of n (0.43) reported elsewhere [66]. Nevertheless, in a similar case, an analogous classification was reported previously [67]. For the PLLA–PCL–PEG 4 terpolymer the n value is 0.47, indicating diffusion from a planar matrix. However, for PLLA–PCL–PEG 2, the n value was 0.59, indicating an anomalous transport for a planar matrix. Besides, the analysis through the Korsmeyer–Peppas extended model determined that n value of PLLA–PCL–PEG 2 terpolymer was 0.77, whereas for NC 1 and NC 2, the values were 0.78 and 0.76, respectively, indicating an anomalous transport for a planar matrix. For all these materials, the value of b was 0.12, indicating that the presence of $CNTs_{po}$ has a small influence on the "burst effect." Contrarily, for PLLA–PCL–PEG 4 terpolymer, the value of n was 0.61 and b was 0.89, while for NC 3 and NC 4, the values of n were 0.86 and 0.56, respectively, but for both nanocomposites, the values of b were negative. Due to negative values do not have physical meaning, these results indicate a poor fit.

The fact that methotrexate is poorly water-soluble (approximately 65 μg/mL) [68] favors their distribution on the PCL chains due to the hydrophobic nature of this biopolymer [14]. In this sense, the lower values of ΔH_{m1} for the prepared terpolymers and nanocomposites compared to the $\Delta H_{m\,PCL\,4}$ of pure PCL 4 indicate a reduction in crystallinity, which favors faster hydrolysis of the PCL domains [69] induced by an increment in the mobility of the chains of PCL [70]. This affects the methotrexate release. Although the "burst effect" was not substantially reduced for the studied nanocomposites, it is evident that in the release tests performed with the nanocomposites, the methotrexate release time was extended, which can be a positive factor in considering their possible use.

 doi:10.20944/preprints202408.1347.v1

4. Conclusions

PLLA–PCL–PEG/CNT$_{po}$ nanocomposites were prepared and characterized through DSC as well as FT-IR, ^{1}H-NMR, and XPS spectroscopies to evaluate their ability to act as nanocarriers of methotrexate. CNTs were prepared through CVD, purified, and chemically functionalized to achieve partial oxidation. The content of the carboxyl groups was higher than that of the hydroxyl groups in the CNTs$_{po}$. Wet BD was used as an initiator to prepare a series of linear PLLAs and PCL through ROP. The water in the wet BD acts as an effective co-initiator in the synthesis of these homopolymers. PLLA–PCL copolymers and PLLA–PCL–PEG segmented terpolymers were synthesized using OxCl as an effective linker agent. These terpolymers have strong hydrophobic characteristics due to the high contents of PLLA and PCL blocks. The evidence recorded by FT-IR strongly suggests that the carboxyl and hydroxyl groups of the CNTs$_{po}$ form hydrogen bonding with the ester carbonyl groups of the PCL chains. Moreover, the CNTs$_{po}$ act as nucleating agents of the PCL chains. This suggests that the CNTs$_{po}$ are preferentially oriented to the PCL chains. The XPS measurements indicated the CNTs$_{po}$ are grafted to the PLLA–PCL–PEG terpolymers. For both PLLA–PCL–PEG terpolymers and PLLA–PCL–PEG/CNT$_{po}$ nanocomposites, a "burst release" of methotrexate was detected. The "burst release" was attenuated but was not eliminated for the nanocomposites. The in vitro release behavior was analyzed using five models. For all the nanocomposites, the best fit was obtained with the first-order model, whereas for the PLLA–PCL–PEG 2 and PLLA–PCL–PEG 4 terpolymers, the best fit was determined with the Hixson–Crowell and Korsmeyer–Peppas models, respectively. The analysis conducted with the Korsmeyer–Peppas model revealed that in general, for both the nanocomposites and terpolymers studied Fickian diffusion drives the methotrexate release.

Supplementary Materials: The following supporting information can be downloaded at the website of this paper posted on Preprints.org.

Author Contributions: Karla J. González-Iñiguez: Methodology, Validation, Investigation. **Edgar B. Figueroa-Ochoa:** Formal analysis, Investigation, Writing – Review & Editing. **Antonio Martínez-Richa:** Investigation, Resources, Writing – Review & Editing. **Leonardo R. Cajero-Zul:** Formal analysis, Investigation. **Sergio M. Nuño-Donlucas:** Conceptualization, Resources, Writing - Original Draft, Writing – Review & Editing, Supervision, Project administration, Funding acquisition.

Funding: This research was funded by CONACyT, grant numbers 101369 and 123732.

Institutional Review Board Statement: Not applicable.

Data Availability Statement:. The data presented in this study are available on request from the corresponding author.

Acknowledgments: The authors thank Karla A. Barrera Rivera (Universidad de Guanajuato) for their technical assistance. All authors kindly acknowledge Laboratorio Nacional de Caracterización de Propiedades Fisicoquímicas y Estructura Molecular (Consejo Nacional de Ciencia y Tecnología (CONACYT), grant 123732) for the instrumentation time provided. We also appreciate Saúl Gallegos Castillo (Universidad de Guadalajara) for your support in the Laboratorio de Análisis Industriales y Especiales, as well as Dr. Humberto Gutiérrez Pulido (Universidad de Guadalajara) and Dra. Ruth Padilla Muñoz (Universidad de Guadalajara) for your attendance for using the Instituto Transdisciplinar de Investigación y Servicios (ITRANS). CONACyT funded this research under grant 101369.

Conflicts of Interest: The authors declare no conflicts of interest. The funders had no role in the design of the study; in the collection, analyses, or interpretation of data; in the writing of the manuscript; or in the decision to publish the results.

References

1. Lopes, J.R.; Santos, G.; Barata, P.; Oliveira, R.; Lopes, C.M. Physical and chemical stimuli-responsive drug delivery systems: targeted delivery and main routes of administration. *Curr. Pharm. Des.* **2013,** *19*, 7169-7184.
2. Coelho, J.F.; Ferreira, P.C.; Alves, P.; Cordeiro, R.; Fonseca, A.C.; Góis, J.R.; Gil, M.H. Drug delivery systems: Advances technologies potentially applicable in personalized treatments. *EPMA J.* **2010**, *1*, 164-209.

3. Ulbrich, K.; Holá, K.; Šubr, V.; Bakandritsos, A.; Tuček, J.; Zbořil, R. Targeted drug delivery with polymers and magnetic nanoparticles: covalent and noncovalent approaches, release control, and clinical studies. *Chem. Rev.* **2016**, *116*, 5338-5431.
4. Oladipo, A.O.; Lebelo, S.L.; Msagati, T.A.M. Nanocarrier design-function relationship: The prodigious role of properties in regulation biocompatibility for drug delivery applications. *Chem. Biol. Interact.* **2023,** *377*, 110466.
5. Raquez, J.-M.; Habibi, Y.; Murariu, M.; Dubois, P. Polylactide (PLA)-based nanocomposites. *Prog. Polym. Sci.* **2013**, *38*, 1504-1542.
6. Saska, S.; Pilatti, L.; Blay, A.; Shibli, J.A. Bioresorbable polymers: advanced materials and 4D printing for tissue engineering. *Polymers* **2021**, *13*, 563.
7. Tokiwa, Y.; Jarerat, A. Biodegradation of poly(L-lactide). *Biotechnol. Lett.* **2004**, *26*, 771-777.
8. Sosnowski, S.; Gadzinowski, M.; Slomkowski, S. Poly(L,L-lactide) microspheres by ring-opening polymerization. *Macromolecules* **1996,** *29*, 4556-4564.
9. Brzeziński, M.; Biela, T. Polylactide nanocomposites with functionalized carbon nanotubes and their stereocomplexes: A focused review. *Mater. Lett.* **2014**, 121, 244-250.
10. El Yousfi, R.; Brahmi, R.; Dalli, M.; Achalhi, N.; Azougagh, O.; Tahani, A.; Touzani, R.; El Idrissi, A. Recent advances in nanoparticle development for drug delivery: A comprehensive review of polycaprolactone-based multi-arm architerctures. *Polymers* **2023**, *15*, 1835.
11. Woodruff, M.A.; Hutmacher, D.W. The return of a forgotten polymer -Polycaprolactone in the 21st century. *Prog. Polym. Sci.* **2010**, *35*, 1217-1256.
12. Tambralli, A.; Blakeney, B.; Anderson, J.; Kushwaha, M.; Andukuri, A.; Dean, D.; Jun, H.-W. A hybrid biomimetic scaffold composed of electrospun polycaprolactone nanofibers and self-assembled peptide amphiphile nanofibers. *Biofabrication* **2009**, *1*, 025001.
13. Aghdam, R.M.; Najarian, S.; Shakhesi, S.; Khanlari, S.; Shaabani, K.; Sharifi, S. Investigating the effect of PGA on physical and mechanical properties of electrospun PCL/PGA blend nanofibers. *J. Appl. Polym. Sci.* **2012**, *124*, 123-131.
14. Wang, X.; Wang, Y.; Wei, K.; Zhao, N.; Zhang, S.; Chen, J. Drug distribution within poly(ε-caprolactone) microspheres and in vitro release. *J. Mater. Process. Technol.* **2009**, *209*, 348-354.
15. Constantino, V.R.L.; Figueiredo, M.P.; Magri, V.R.; Eulálio, D.; Cunha, V.R.R.; Alcântara, A.C.S.; Perotti, G.F. Biomaterials based on organic polymers and layered double hydroxides nanocomposites: drug delivery and tissue engineering. *Pharmaceutics* **2023**, *15*, 413.
16. Yadav, D.; Dewangan, H.K. PEGYLATION: an important approach for novel drug delivery system. *J. Biomater. Sci. Polym. Ed.* **2021**, *32*, 266-280.
17. Veronese, F.M.; Pasut, G. PEGylation, successful approach to drug delivery. *Drug Discov. Today* **2005**, *10*, 1451-1458.
18. Tian, H.; Tang, Z.; Zhuang, X.; Chen, X.; Jing, X. Biodegradable synthetic polymers: preparation, functionalization and biomedical application. *Prog. Polym. Sci.* **2012**, *37*, 237-280.
19. Tamboli, V.; Mishra, G.P.; Mitra, A.K. Novel pentablock copolymer (PLA-PCL-PEG-PCL-PLA) based nanoparticles for controlled drug delivery: Effect of copolymer compositions on the crystallinity of copolymers and in vitro drug release profile from nanoparticles. *Colloid Polym. Sci.* **2013**, *291*, 1235-1245.
20. Ramasamy, T.; Ruttala, H.B.; Gupta, B.; Poudel, B.K.; Choi, H.-G.; Yong, C.S.; Kim, J.O. Smart chemistry-based nanosized drug delivery systems for systemic applications: A comprehensive review. *J. Control. Release* **2017**, *258*, 226-253.
21. Celentano, W.; Pizzocri, M.; Moncalvo, F.; Pessina, F.; Matteoli, M.; Cellesi, F.; Passoni, L. Functional poly(ε-caprolactone)/poly(ethylene glycol) copolymers with complex topologies for doxorubicin delivery to a proteinase-rich tumor environment. *ACS Appl. Polym. Mater.* **2022**, *4*, 8043-8056.
22. Rad, A.H.; Asiaee, F.; Jafari, S.; Shayanfar, A.; Lavasanifar, A.; Molavi, O. Poly(ethylene glycol)-poly(ε-caprolactone)-based micelles for solubilization and tumor-targeted delivery of silibinin. *Bioimpacts* **2020**, *10*, 87-95.
23. Chu, B.; Zhang, L.; Qu, Y.; Chen, X.; Peng, J.; Huang, Y.; Qian, Z. Synthesis, characterization and drug loading property of monomethoxy-poly(ethylene glycol)-poly(ε-caprolactone)-poly(D,L-lactide) (MPEG-PCLA) copolymers. *Sci. Rep.* **2016**, *6*, 34069.
24. Jikei, M.; Takeyama, Y.; Yamadoi, Y.; Shinbo, N.; Matsumoto, K.; Motokawa, M.; Ishibashi, K.; Yamamoto, F. Synthesis and properties of poly(L-lactide)-poly(ε-caprolactone) multiblock copolymers by self-polycondensation of diblock macromonomers. *Polym. J.* **2015**, *47*, 657-665.
25. Zhu, X.; Liu, C.; Duan, J.; Liang, X.; Li, X.; Sun, H.; Kong, D.; Yang, J. Synthesis of three-arm block copolymer poly(lactic-co-glycolic acid)-poly(ethylene glycol) with oxalyl chloride and its application in hydrophobic drug delivery. *Int. J. Nanomedicine* **2016**, *11*, 6065-6077.
26. Jia, W.; Gu, Y.; Gou, M.; Dai, M.; Li, X.; Kan, B.; Yang, J.; Song, Q.; Wei, Y.; Qian, Z. Preparation of biodegradable polycaprolactone/poly(ethylene glycol)/polycaprolactone (PCEC) nanoparticles. *Drug Deliv.* **2008**, *15*, 409-416.

 doi:10.20944/preprints202408.1347.v1

27. Huang, X.; Brazel, C.S. On the importance and mechanisms of burst release in matrix-controlled drug delivery systems. *J. Control. Release* **2001**, *73*, 121-136.
28. Qnouch, A.; Solarczyk, V.; Verin, J.; Tourrel, G.; Stahl, P.; Danede, F.; Willart, J.F.; Lemesre, P.E.; Vincent, C.; Siepmann, J.; Siepmann, F. Dexamethasone-loaded cochlear implants: How to provide a desired "burst release". *Int. J. Pharm. X.* **2021**, *3*, 100088.
29. Bakhrushina, E.O.; Sakharova, P.S.; Konogorova, P.D.; Pyzhov, V.S.; Kosenkova, S.I.; Bardakov, A.I.; Zubareva, I.M.; Krasnyuk, I.I.; Krasnyuk Jr., I.I. Burst release from in situ forming PLGA-based implants: 12 effectors and ways of correction. *Pharmaceutics* **2024**, *16*, 115.
30. Li, J.; Yap, S.Q.; Yoong, S.L.; Nayak, T.R.; Chandra, G.W.; Ang, W.H.; Panczyk, T.; Ramaprabhu, S.; Vashist, S.K.; Sheu, F.-S.; Tan, A.; Pastorin, G. Carbon nanotube bottles for incorporation, release and enhanced cytotoxic effect of cisplatin. *Carbon* **2012**, *50*, 1625-1634.
31. Heister, E.; Neves, V.; Lamprecht, C.; Silva, S.R.P.; Coley, H.M.; McFadden, J. Drug loading, dispersion stability, and therapeutic efficacy in targeted drug delivery with carbon nanotubes. *Carbon* **2012**, *50*, 622-632.
32. Ye, L.; Chen, W.; Chen, Y.; Qiu, Y.; Yi, J.; Li, X.; Lin, Q.; Guo, B. Functionalized multiwalled carbon nanotube-ethosomes for transdermal delivery of ketoprofen: Ex vivo and in vivo evaluation. *J. Drug Deliv. Sci. Technol.* **2022**, *69*, 103098.
33. Liu, Z.; Tabakman, S.; Welsher, K.; Dai, H. Carbon nanotubes in biology and medicine: In vitro and in vivo detection, imaging and drug delivery. *Nano Res.* **2009**, *2*, 85-120.
34. Lee, W.J.; Clancy, A.J.; Fernández-Toribio, J.C.; Anthony, D.B.; White, E.R.; Solano, E.; Leese, H.S.; Vilatela, J.J.; Shaffer, M.S.P. Interfacially-grafted single-walled carbon nanotube/poly(vinyl alcohol) composite fibers. *Carbon* **2019**, *146*, 162-171.
35. Silva-Jara, J.M.; Manríquez-González, R.; López-Dellamary, F.A.; Puig, J.E.; Nuño-Donlucas, S.M. Semi-continuous heterophase polymerization to synthesize nanocomposites of poly(acrylic acid)-functionalized carbon nanotubes. *J. Macromol. Sci. Part A* **2015**, *52*, 732-744.
36. Sandoval-García, K.; Alvarado-Mendoza, A.G.; Jiménez-Avalos, J.A.; García-Carvajal, Z.Y.; Olea-Rodríguez, M.A.; Cajero-Zul, L.R.; Nuño-Donlucas, S.M. Synthesis, characterization and evaluation of the toxicity, drug release ability and antibacterial capacity of nanocomposites of polyethylene glycol and functionalized carbon nanotubes. *J. Macromol. Sci. Part A* **2022**, *59*, 889-903.
37. Xia, R.; Li, M.; Zhang, Y.; Qian, J.; Yuan, X. Surface modification of MWNTs with BA-MMA-GMA terpolymer by single-step grafting technique. *J. Appl. Polym. Sci.* **2011**, *119*, 282-289.
38. Villar-Alvarez, E.; Figueroa-Ochoa, E.; Barbosa, S.; Soltero, J.F.A.; Taboada, P.; Mosquera, V. Reverse poly(butylene oxide)-poly(ethylene oxide)-poly(butylene oxide) block copolymers with lengthy hydrophilic blocks as efficient single and dual drug-loaded nanocarriers with synergistic toxic effects on cancer cells. *RSC Adv.* **2015**, *5*, 52105-52120.
39. Storey, R.F.; Taylor, A.E. End-group analysis of poly(e-caprolactone) initiated with water, ethylene glycol, and 1,4-butanediol. *J. Macromol. Sci. Part A* **1996**, *33*, 77-89.
40. Abdolmaleki, A.; Mallakpour, S.; Rostami, M. Development of carboxylated multi-walled carbon nanotubes reinforced potentially biodegradable poly(amide-imide) based on *N*-trimellitylimido-S-valine matrixes: Preparation, processing, and thermal properties. *Prog. Org. Coat.* **2015**, *80*, 71-76.
41. Alghunaim, N.S. Optimization and spectroscopic studies on carbon nanotubes/PVA nanocomposites. *Results Phys.* **2016**, *6*, 456-460.
42. Omran, S.M.; Abdullah, E.T.; Al-Zuhairi, O.A. Structural and infrared spectroscopy of polyvinylpyrrolidone/multi-walled carbon nanotubes nanocomposite. *Iraqi J. Phys.* **2021**, *19*, 1-6.
43. Parada, L.G.; Cesteros, L.C.; Meurio, E.; Katime, I. Miscibility and specific interactions in blends of poly(vinyl acetate-co-vinyl alcohol) with poly(ethyloxazoline), *Macromol. Chem. Phys.* **1997**, *198*, 2505-2517.
44. Antolín-Cerón, V.H.; Gómez-Salazar, S.; Soto, V.; Ávalos-Borja, M.; Nuño-Donlucas, S.M. Polymer nanocomposites containing carbon nanotubes and miscible polymer blends based on poly[ethylene-co-(acrylic acid)], *J. Appl. Polym. Sci.* **2008**, *108*, 1462-1472.
45. AAnalyzer®: A Peak-Fitting Program for Photoemission Data. Available online: https://xpsoasis.org/.
46. Ratner, B.D.; Castner, D.G. Electron spectroscopy for chemical analysis. In: *Surface Analysis: The Principal Techniques*, 2nd ed.; Vickerman, J.C., Gilmore, I.S., Eds.; Wiley: Chichester, UK, 2009, pp. 53-79.
47. Beamson, G.; Briggs, D. *High Resolution XPS of Organic Polymers: The Scienta ESCA300 Database*, 1st ed.; Wiley: Chichester, UK, 1992, pp. 84-45, 136-137, 142-143.
48. Wingrove, A.S.; Caret, R.L. *Organic chemistry*, 1st ed.; Harla: Ciudad de Mexico, MX, 1984, pp. 1103-1104.
49. Bogdanov, B.; Vidts, A.; Van Den Buicke, A.; Verbeeck, R.; Schacht, E. Synthesis and thermal properties of poly(ethylene glycol)-poly(ε-caprolactone) copolymers. *Polymer* **1998**, *39*, 1631-1636.
50. Bogdanov, B.; Vidts, A.; Schacht, E.; Berghmans, H. Isothermal crystallization of poly(ε-caprolactone-ethylene glycol) block copolymers. *Macromolecules* **1999**, *32*, 726-731.

 doi:10.20944/preprints202408.1347.v1

51. Takeshita, H.; Fukumoto, K.; Ohnishi, T.; Ohkubo, T.; Miya, M.; Takenaka, K.; Shiomi, T. Formation of lamellar structure by competition in crystalization of both components for crystalline-crystallines block copolymers. *Polymer* **2006**, *47*, 8210-8218.
52. Xu, Y.; He, Y.; Wei, J.; Fan, Z.; Li, S. Morphology and melt crystallization of PCL-PEG diblocj copolymers. *Macromol. Chem. Phys.* **2008**, *209*, 1836-1844.
53. Sun, J.; He, C.; Zhuang, X.; Jing, X.; Chen, X. The crystallization behavior of poly(ethylene glycol)-poly(ε-caprolactone) diblock copolymers with asymmetric block compositions. *J. Polym. Res.* **2011**, *18*, 2161-2168.
54. Shokrolahi, F.; Yeganeh, H. Soft segment composition and its influence on phase-separated morphology of PCL/PEG-based poly(urethane urea)s. *Iran Polym. J.* **2014**, *23*, 505-512.
55. Xu, Y.; Zhang, Y.; Fan, Z.; Li, S. Melt crystallization and morphology of poly(ε-caprolactone)-poly(ethylene glycol) diblock copolymers with different compositions and molecular weights. *J. Polym. Sci. Part B: Polym Phys*. **2010**, *48*, 289-293.
56. Flory, A.L.; Ramanathan, T.; Brinson, L.C. Physical aging of single wall carbon nanotube polymer nanocomposites: effect of functionalization of the nanotube on the enthalpy relaxation. *Macromolecules* **2010**, *43*, 4247-4252.
57. Babal, A.S.; Gupta, R.; Singh, B.P.; Dhakate, S.R. Depression in glass transition temperature of multiwalled carbon nanotubes reinforced polycarbonate composites: Effect of functionalization. *RSC Adv.* **2015**, *5*, 43462-43472.
58. Saldaña-Rojas, U.A.; Cortés-Llamas, S.A.; Jiménez-Avalos, J.A.; García-Carvajal, Z.Y.; Olea-Rodríguez, M.A.; Cajero-Zul, L.R.; Nuño-Donlucas, S.M. Evaluation of the toxicity and cisplatin drug release ability of nanocomposites of polyethylene glycol and carbon nanotubes functionalized with Zn^{2+} ions. *Int. J. Polym. Mater.* **2024**, *73*, 946-960.
59. Wang, H.; Xu, J.; Wang, J.; Chen, T.; Wang, Y.; Tan, Y.W.; Su, H.; Chan, K.L.; Chen, H. Probing the kinetics of short-distance drug release from nanocarriers to nanoacceptors. *Angew. Chem. Int. Ed.* **2010**, *49*, 8426-8430.
60. Korsmeyer, R.W.; Gumy, R.; Doelker, E.; Buri, P.; Peppas, N.A. Mechanisms of solute release from porous hydrophilic polymers. *Int. J. Pharm.* **1983**, *15*, 25-35.
61. Kim, H.; Fassihi, R. Application of binary polymer in drug release rate modulation. 2. Influence of formulation variables and hydrodynamic conditions on release kinetics. *J. Pharm. Sci.* **1997**, *86*, 323-328.
62. Polli, J.E.; Rekhi, G.S.; Augsburger, L.L.; Shah, V.P. Methods to compare dissolution profiles and a rationale for wide dissolution specifications for metoprolol tartrate tablets. *J. Pharm. Sci*. **1997**, *86*, 690-700.
63. Hixson, A.W.; Crowell, J.H. Dependence of reaction velocity upon surface and agitation. *Ind. Eng. Chem.* **1931**, *23*, 923-931.
64. Zhang, Y.; Huo, M.; Zhou, J.; Zou, A.; Li, W.; Yao, C.; Xie, S. DDSolver: An add-in program for modeling and comparison of drug dissolution profiles. *AAPS J.* **2010**, *12*, 263-271.
65. Mayer, B.X.; Mensik, C.; Krishnaswami, S.; Hartmut, D.; Eichler, H.–G.; Schmetterer, L.; Wolzt, M. Pharmacokinetic-pharmacodynamic profile of systemic nitric oxide-synthase inhibition with L-NMMA in humans. *Br. J. Clin. Pharmacol*. **1999**, *47*, 539-544.
66. Bruschi, M.L. Mathematical models of drug release. In *Strategies to modify the drug release from pharmaceutical systems*, 1st ed.; Bruschi, M.L., Ed.; Elsevier: Cambridge, UK, 2015, pp. 63-86.
67. Shoaib, M.H.; Tazeen, J.; Merchant, H.A.; Yousuf, R.I. Evaluation of drug release kinetics from ibuprofen matrix tablets using HPMC. *Pak. J. Pharm. Sci.*, **2006**, *19*, 119-124.
68. Giri, B.R.; Kim, J.S.; Park, J.H.; Jin, S.G.; Kim, K.S.; Din, F.U.; Choi, H.G.; Kim, D.W. Improved bioavailability and high photostability of methotrexate by spray-dried surface-attached solid dispersion with and aqueous medium. *Pharmaceutics* **2021**, *13*, 111.
69. Erdal, N.B.; Lando, G.A.; Yadav, A.; Srivastava, R.K.; Hakkarainen, M. Hydrolytic degradation of porous crosslinked poly(e-caprolactone) synthesized by high internal phase emulsion templating. *Polymers* **2020**, *12*, 1849.
70. Yoshioka, T.; Kamada, F.; Kawazoe, N.; Tateishi, T.; Chen, G. Structural changes and biodegradation of PLLA, PCL, and PLGA sponges during in vitro incubation. *Polym. Eng. Sci.* **2010**, *50*, 1895-1903.